PERGAMON

Journal of Structural Geology 26 (2004) 377–398

JOURNAL OF STRUCTURAL GEOLOGY

www.elsevier.com/locate/jsg

Fault scaling relationships, deformation rates and seismic hazards: an example from the Lazio–Abruzzo Apennines, central Italy

Gerald P. Roberts[a,*], Patience Cowie[b], Ioannis Papanikolaou[a], Alessandro M. Michetti[c]

[a]*The Research School of Geological and Geophysical Sciences, Birkbeck College and University College London, Gower Street, London WC1E 6BT, UK*
[b]*Department of Geology and Geophysics, The University of Edinburgh, West Mains Road, Edinburgh EH9 3JW, UK*
[c]*Universita dell'Insubria, Dipartimento di Scienze, CC.FF.MM., Via Lucini, 3, 22100, Como, Italy*

Received 5 January 2001; accepted 28 April 2003

Abstract

Spatial variations in the number of seismic shaking events in a given time period (frequency) implied by measured throw-rates associated with active normal faults in central Italy are investigated through comparison with models of fault growth and the historical record of earthquake shaking for the region. Measured offsets of 18 ka glacial features provide a throw-rate database averaged over a time period much longer than the reliable portion of the historical earthquake record for the region (<ca. 1 ka). Throw-rates are greatest in the centre of the studied fault array and show a six-fold decrease from central to distal faults, implying spatial variations in the frequency of seismic shaking events. We attempt to validate these observations by comparing them with throw-rates predicted by a calculation that takes into account the growth patterns of normal fault systems that exhibit well-known scaling relationships between fault length and throw. We also convert the measured throw-rates into a map of implied frequency of seismic shaking events and attempt to validate the map by comparing it with the probably complete records of seismic shaking since 1349 A.D. that exist for 14 towns in the region. Our results confirm that the throw-rate database is compatible with both the record of historical seismic shaking and what we know about the growth of normal faults. The results imply that knowledge of fault scaling parameters and geological determined deformation rates are valuable tools in seismic hazard assessment.

Keywords: Fault scaling relationships; Deformation rates; Seismic hazards

1. Introduction

The rate at which a fault slips fundamentally determines the seismic hazard that it represents because average earthquake recurrence intervals tend to decrease as slip rates increase. Measuring slip-rates is difficult using only historical earthquake data if the recurrence interval for large earthquakes (>Ms 6.0) on a given fault is longer than the historical record of earthquakes for that fault. This problem is particularly pertinent in low strain rate extensional settings where recurrence intervals for large events on particular active normal faults are measured in hundreds to thousands of years. The problem is exacerbated if earthquake sequences on a given fault exhibit temporal clustering, because the slip-rates should then be averaged over a time period containing a large number of seismic cycles on that fault. Slip-rate data averaged over many earthquake cycles on a particular fault will clearly have to be derived from the offsets of geological features of known age because of the long time periods involved. However, how does one judge the reliability of such multi-earthquake fault-specific slip-rate databases? Long-term (multi-earthquake) slip-rates do not always agree with short-term measurements such as those derived from seismic moment summations of the last ca. 100 years of instrumental earthquake data or geodetic measurements (e.g. Cowie and Roberts, 2001), yet short-term deformation rate data are used to assess seismic hazards (e.g. Clarke et al., 1997). It is unlikely, in our view, that a seismic hazard assessment based on one slip-rate data set will be taken seriously if a conflicting dataset exists. Another point is that the slip-rates themselves do not convey the spatial variation in the intensity of seismic shaking or how often such events occur

* Corresponding author. Tel.: +44-20-76797713; fax: +44-20-73830008.
E-mail address: gerald.roberts@ucl.ac.uk (G.P. Roberts).

0191-8141/$ - see front matter © 2003 Elsevier Ltd. All rights reserved.
doi:10.1016/S0191-8141(03)00104-4

(frequency). To provide such a seismic hazard assessment, the slip-rate must (1) first be converted into an equivalent number of earthquakes of given magnitude from a given magnitude–frequency distribution, and (2) the spatial effects in terms of shaking for each putative earthquake must be considered.

This paper provides a case study of an attempt to validate a throw-rate database (vertical component of slip) from Roberts and Michetti (2003, this issue) and use it in mapping both the intensity and frequency of seismic shaking events for given time period.

The area to be studied is the Lazio–Abruzzo Apennines in central Italy, which is actively extending and has suffered very damaging normal faulting earthquakes (e.g. the 1915 Fucino earthquake, ca. Ms 6.9–7.0, 33,000 fatalities; 1984 Abruzzo earthquakes, Ms 5.8, 10 fatalities) some of which are strongly felt in the capital city of Rome (Michetti et al., 1996). The high mountains of Lazio–Abruzzo were sparsely-populated during parts of the last two millennia and earthquake records prior to the Roman period are certainly incomplete (e.g. Pantosti et al., 1996). Thus, a complete record of all large magnitude earthquakes may only be available for ca. 1000 years or much less. However, there is evidence to suggest that at least 14 towns in the region have a complete record of earthquake shaking stretching back to 1349 A.D., a time when large earthquakes struck the region. The historical record for these towns can be retrieved from a website of the Istituto Nazionale di Geofisica e Vulcanologia (INGV 1). These towns either record the 1349 A.D. earthquake or have records of earlier events. They also have numerous records of shaking even for small shaking intensity values indicating that they have been continuously monitored since 1349 A.D. to an extent that it is unlikely that large earthquakes have been missed. However, this record does not detail which fault ruptured to produce the recorded shaking. A fault-specific record of historical and pre-historical earthquakes is, however, in part provided by palaeoseismological studies on some of the active faults. Fault-specific earthquake return times measured from different palaeoseismological sites across the Lazio–Abruzzo Apennines range between ca. 500– $>$ 3000 years (Giraudi and Frezzotti, 1995; Michetti et al., 1996; Pantosti et al., 1996; Galadini et al., 1997). With only 653 years elapsed since 1349 A.D. and the aforementioned fault-specific recurrence intervals, the historical shaking record almost certainly does not include rupture of every fault in the region. To map the spatial variation in seismic shaking hazard, that is, the spatial variation in fault slip-rates, a longer-term record, which includes slip on every active fault in the region, is needed. Roberts and Michetti (2003) provide a throw-rate (vertical component of the slip-rate) database for the area which includes profiles of spatial throw-rate variation along what they claim to be all or most of the active faults in the region. The throw-rates are derived from offset late-glacial features (18 ka) and so average the throw-rate over a large number of earthquake cycles on each fault. Roberts and Michetti (2003, this issue) show that for the last 18 kyrs, maximum throw rates for individual active normal faults show a ca. six-fold increase from the NW and SE edges to the centre of the region, implying spatial variation in the frequency of seismic shaking events. It is this long-term (i.e. multi-earthquake), fault-specific throw-rate database that we seek to validate. We also wish to quantify the implied spatial variation in frequency of seismic shaking events of given intensity. Specifically, our aim is to see if the record of shaking for the 14 towns mentioned above can be post-dicted using the throw-rate database of Roberts and Michetti (2003).

The paper is divided into two main sections. First, we compare the throw-rate database for central Italy (Roberts and Michetti, 2003) with what one would expect for a fault system adhering to scaling relationships between the lengths and displacements on faults. Cowie and Roberts (2001) show that the active fault spacing and the spatial variation in throw-rates within an array of faults should be to some extent predictable given knowledge of the along-strike positions, lengths and finite throws of faults within the array. Thus the comparison allows the throw-rate database to be validated to some extent; a further validation is carried out in the second part of the paper (see below). Second, we calculate the number of earthquakes needed to produce the measured pattern of 18 kyrs throw and also calculate the spatial variation in the intensity and frequency of seismic shaking events implied by this suite of putative earthquakes. We do this by using empirical relationships between rupture lengths, earthquake magnitudes, slip on surface ruptures and the sizes of given isoseismals. The results are displayed as a new type of seismic hazard map. An attempt to validate the map is made by comparing it with the historical record of seismic shaking for the 14 aforementioned towns in the region which, in effect, is also a second way of validating the throw-rate database (see above). Because the method of Cowie and Roberts (2001) produces an independent throw-rate estimation, we also produce a spatial variation in the intensity and frequency of seismic shaking events map using our predictions of what the throw-rate ought to be given knowledge of the fault scaling parameters of the fault array in question. In turn, we compare these independent results with the historical record of seismic shaking for the region.

Our results show that the intensities and frequencies of seismic shaking calculated using the throw-rate database of Roberts and Michetti (2003) and the independent throw-rate database provided by the method of Cowie and Roberts (2001) are very similar. They are also similar to the values recorded in the historical record of earthquake shaking for the region. To our knowledge, this is the first time that the spatial variation in intensity and frequency of seismic shaking events has been post-dicted with a reasonable degree of success for a low strain-rate normal fault system using (a) a throw-rate database measured from offset 18 ka geology, and (b) scaling relationships between the lengths, positions and displacements on faults which predict how

slip has accumulated over time periods of 10^5–10^6 years (see Cowie and Roberts, 2001). We discuss how our results may be used to predict future patterns of earthquake shaking.

First, we summarise how scaling relationships can be used to predict active fault spacings and throw-rates on individual faults (Cowie and Roberts, 2001) (Section 2). Second, we attempt to predict measured active fault spacings in the Lazio–Abruzzo Apennines using scaling relationships (Section 3). Third, we attempt to predict measured throw-rates on individual active faults in the Lazio–Abruzzo Apennines using scaling relationships (Section 4), and compare these with measured values from Roberts and Michetti (2003). Finally, before our discussion and conclusions we produce hazard maps from our measured and predicted throw-rates, and compare our results with the historical record of seismic shaking (Section 5).

2. Scaling relationships and deformation rates

Cowie and Roberts (2001) suggest that the total throws, throw-rates and across strike spacings of active normal faults develop in accordance with what we know of fault scaling parameters (Fig. 1). The length of a fault (L) scales with its maximum displacement (d) in the form $d = \gamma L$. Given that the 2–3 orders of magnitude variation in γ is small compared with the eight orders of magnitude in fault length included in the global

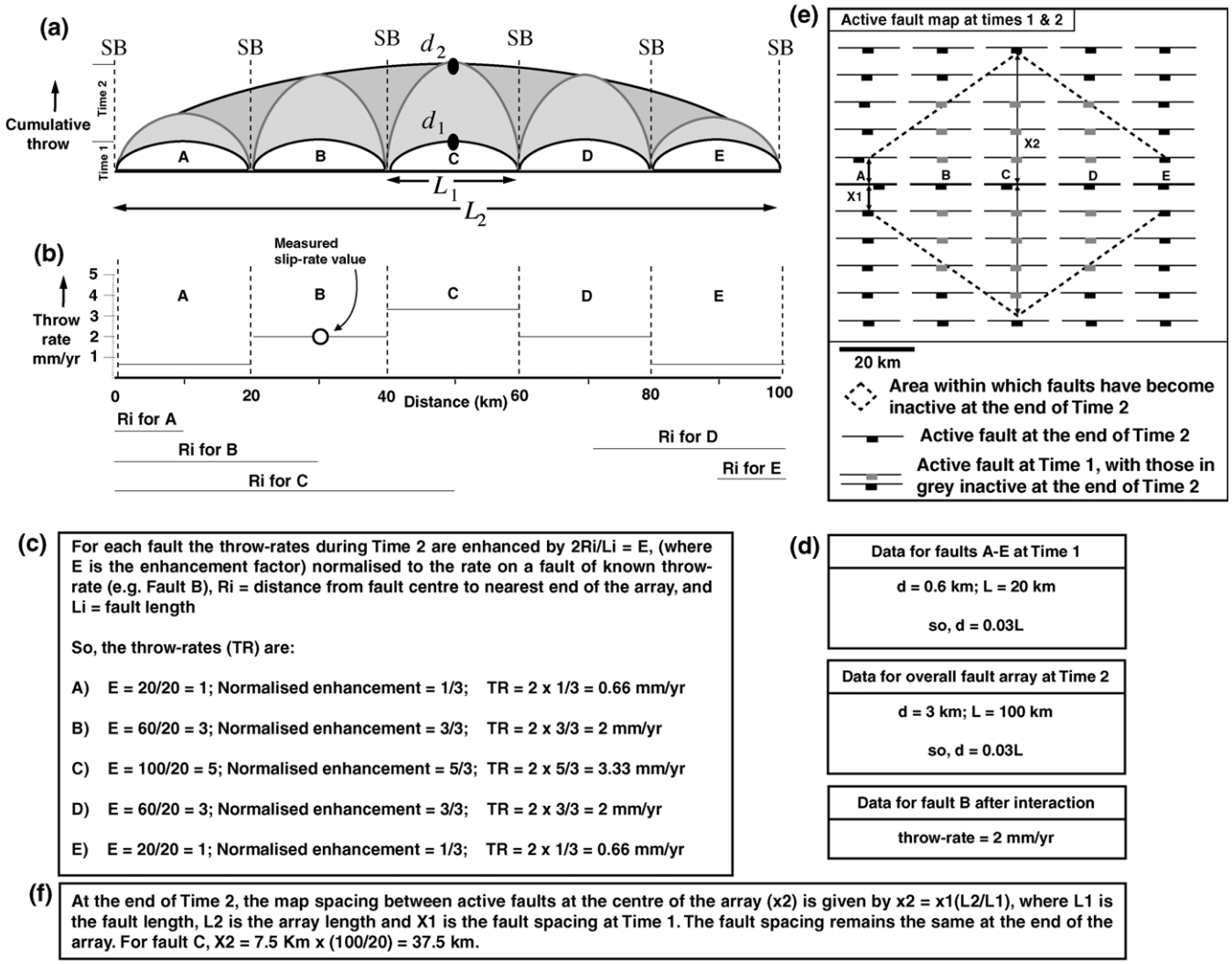

Fig. 1. Growth model and deformation rate assessment procedure for evolving fault systems. (a) Fault growth model for a soft-linked fault system like that in the Lazio–Abruzzo Apennines. The throw-rates must increase towards the centre of the array simply because the fault array ($d_2 = \gamma L_2$) is self-similar with the individual faults ($d_1 = \gamma L_1$), and the fault array develops through interaction between individual faults (see Roberts and Michetti (2003)) for a similar diagram illustrating hard-linked fault systems). (b) Predicted maximum growth rates for the five faults in (a) derived the relationship $E = 2Ri/Li$ (see text for explanation). The relative throw-rate enhancement factors have been normalised to a hypothetical measured value for fault B. (c) and (d) show the data and calculations used in (b). (e) Hypothetical map of active and inactive faults for a region containing faults A–E at the ends of Stage 1 and Stage 2 shown in (a). (f) Data and calculations used in (e).

Table 1
Predicted and measured throw-rates for active faults in the Lazio–Abruzzo Apennines. Measured throw-rates from Roberts and Michetti (2003, this issue)

Fault	*Li*	2*Ri*	2*Ri*/*Li*	Normalised	Predicted rates	Predicted rates × 0.5, 0.33 or 1	Notes	Measured Throw-rate (±0.2 mm/yr)
Rieti	24	24	1.00	0.25	0.49	0.25	>50% overlap with Leonessa with ca. 8 km spacing	0.40
Leonessa	20	30	1.50	0.37	0.74	0.37	>50% overlap with Rieti with ca. 8 km spacing	0.40
Sella di Corno	25	64	2.56	0.63	1.26	0.63	>50% overlap with Barete with ca. 12 km spacing	0.33
Fiamignano	28	85	3.04	0.75	1.50	0.75	>50 % overlap with Carsoli with ca. 13 km spacing	0.83
Carsoli	25	95	3.80	0.94	1.87	0.62	>50% overlap with Fiamignano and Scurcola with ca. 13 and ca. 8 km spacings, respectively	0.38
Scurcola	35	116	3.31	0.82	1.63	0.82	>50% overlap with Carsoli with ca. 7 km spacing	0.83
Fucino	36	146	4.06	1.00	2.00	2.00	No fault centre within 15 km across strike	2.00
Liri	40	139	3.48	0.86	1.71	0.86	>50% overlap with Trassaco with ca. 7 km spacing	1.10
Trassaco	31	116	3.74	0.92	1.84	0.92	>50% overlap Liri with ca. 7 km spacing	0.83
Pescasseroli	22	86	3.91	0.96	1.93	0.96	>50% overlap with Cinque Miglia with ca. 12 km spacing	0.83
Cassino	31	31	1.00	0.25	0.49	0.49	No fault centre within 15 km across strike	0.33
Barete	22	68	3.09	0.76	1.52	0.76	>50% overlap with Sella di Corno with ca. 12 km spacing	0.55
L'Aquila	37	112	3.03	0.75	1.49	0.75	>50% overlap with Campo Imperatore with ca. 12 km spacing	1.38
Campo Imperatore	26	124	4.77	1.17	2.35	1.17	>50% overlap with L'Aquila with ca. 12 km spacing	1.10
Sulmona	24	124	5.17	1.27	2.55	1.27	>50% overlap with Maiella with ca. 7 km spacing	1.10
Cinque Miglia	20	80	4.00	0.99	1.97	0.99	>50% overlap with Pescasseroli with ca. 12 km spacing	0.38
Maiella	22	108	4.91	1.21	2.42	1.21	>50% overlap with Sulmona with ca. 7 km spacing	0.83

Values are normalised to the Fucino fault.

databases of $d - L$ ratios (e.g. Schlische et al., 1996), large faults are essentially self-similar with the small faults that have linked to form them. Thus, the central portions of a large fault formed through linkage must slip more rapidly than more distal portions in order for it to develop a total slip value that is concomitant with its length (see examples in Cowie and Roberts (2001)). The increase in size of a fault as it links with other faults and increases its displacement also means that it accommodates more strain (Kostrov, 1974). Other faults located across strike must therefore decrease in activity if constant regional strain-rates are to be maintained (Nicol et al., 1997; Cowie, 1998). The above effects also occur for soft-linked faults because triggering of slip by earthquakes on neighbouring faults (e.g. Hodgkinson et al., 1996) causes throw-profile readjustment so that faults located centrally within a soft-linked array develop larger displacements than their more distal faults (e.g. Machette et al., 1991; Cowie, 1998). Eventually, displacements on central faults are concomitant with the length of the soft-linked but interacting array (Cowie and Roberts, 2001).

Cowie and Roberts (2001) use the above to show that relative values for the total throws and throw-rates, and across strike spacings of active normal faults can be predicted if the map patterns of fault traces are well known. The spatial variation in enhancement factors (E) for throw-rates on faults in an interacting array which has a triangular throw profile can be calculated using the relationship $2Ri/Li$, where Li is the length of the ith fault and Ri is the distance between the fault midpoint and the nearest tip of the overall array (Cowie and Roberts, 2001) (Fig. 1). The spacing of active faults (x_2) when the deformation has produced a new large fault through linkage/interaction of smaller faults is given by $x_1(L_2/L_1)$ where x_1 is the average fault spacing between the initial faults of length L_1 and L_2 is the length of the new larger fault (Cowie and Roberts, 2001). However, x_2 is only achieved when the slip on the new larger fault achieves a displacement concomitant with its length ($d_2 = \gamma L_2$). Active fault spacing will be between x_1 and x_2 prior to this time. The implied deformation rate patterns will persist for the entire history of fault slip after interaction/linkage occurs (10^5–10^6 years) (Cowie and Roberts, 2001), presumably with short-lived fluctuations in rate due to temporal earthquake clustering.

The values in Table 1 can be used to perform such calculations for the Lazio–Abruzzo Apennines (Sections 3 and 4). In Sections 3 and 4 we test whether the above calculations can predict the measured six-fold increase in deformation rates from the NW and SE edges to the centre of the region, and the close across-strike spacing (7–15 km) of active faults (Roberts and Michetti, 2003, this issue).

3. Fault scaling and the spacing of active faults in the Lazio–Abruzzo Apennines

First, we examine the observation that across-strike active fault spacings are as small as 7–15 km (Fig. 2). Throw-length profiles (see Roberts and Michetti, 2003, this issue, their Fig. 8) show individual faults that have throw/length ratios of 0.035–0.083. The overall array (L_2 value of 155 km) achieves a throw/length ratio of 0.042, but only if throw values are summed between six parallel faults (6.6 km) spread across over a distance of 50 km, that is, about a third of the entire fault array length (see Roberts and Michetti, 2003, this issue, their Fig. 10). This is not a fair comparison with other throw/length or d/L ratios measured world-wide, which sum values across distances that are only a few percent of the fault length. Thus, for the overall array, we choose the largest throw on a centrally-located fault (2.2 km associated with the Fucino Fault) that we can achieve without summing across strike for distances greater than a few percent of the length of the array. If calculated using only this value for maximum throw, the throw/length ratio is 0.014. The value of 0.014 is less than measured for individual faults (0.035–0.083) as in Fig. 1. Thus, there is no localised fault system that has re-adjusted its throw profile from d_1 to d_2 spanning the

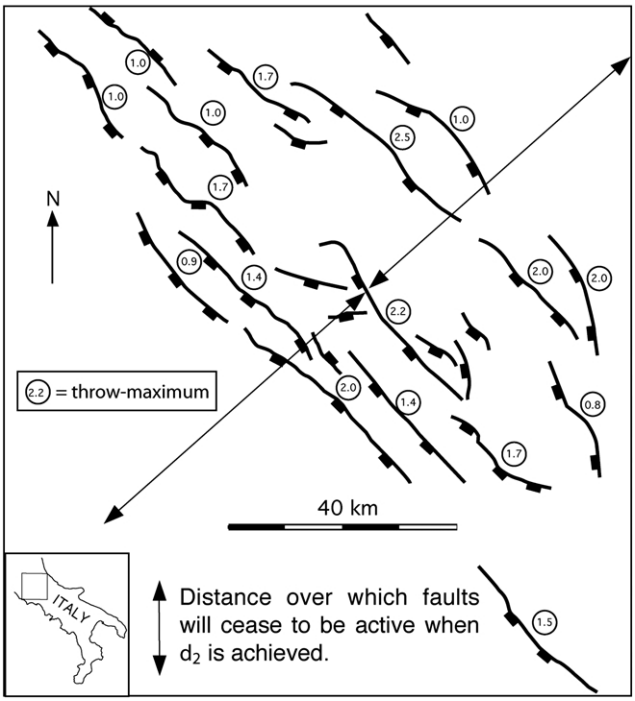

Fig. 2. Map of active faults in the Lazio–Abruzzo Apennines, central Italy from Roberts and Michetti (2003, this issue). The map also shows the across-strike distance within which faults will cease to be active (x_2) if the central Fucino Fault achieves d_2 (see Fig. 1 for reasoning). The Fucino fault has not achieved d_2 so the across-strike fault spacing remains close to x_1.

along-strike length of the Lazio–Abruzzo Apennines, so the across-strike fault spacing should be less than x_2 and probably close to x_1. For faults of $L_1 = 30$ km and $L_2 = 155$ km, x_2 at the centre of the array should be ca. 77.5 km, taking x_1 to be 15 km (Fig. 2). That the active fault spacing is still ca. 7–15 km is consistent with, and we think explained by, the underdisplaced nature of the array (throw/length = 0.014).

4. Calculating absolute deformation rates for individual faults using scaling relationships

We now predict how deformation rates should vary along the strike of the fault array in the Lazio–Abruzzo Apennines using the reasoning in Fig. 1. A fault located in the centre of an array ($d_1 = \gamma L_1$) that links/interacts with others in the array to form a longer system ($d_2 = \gamma L_2$ for the

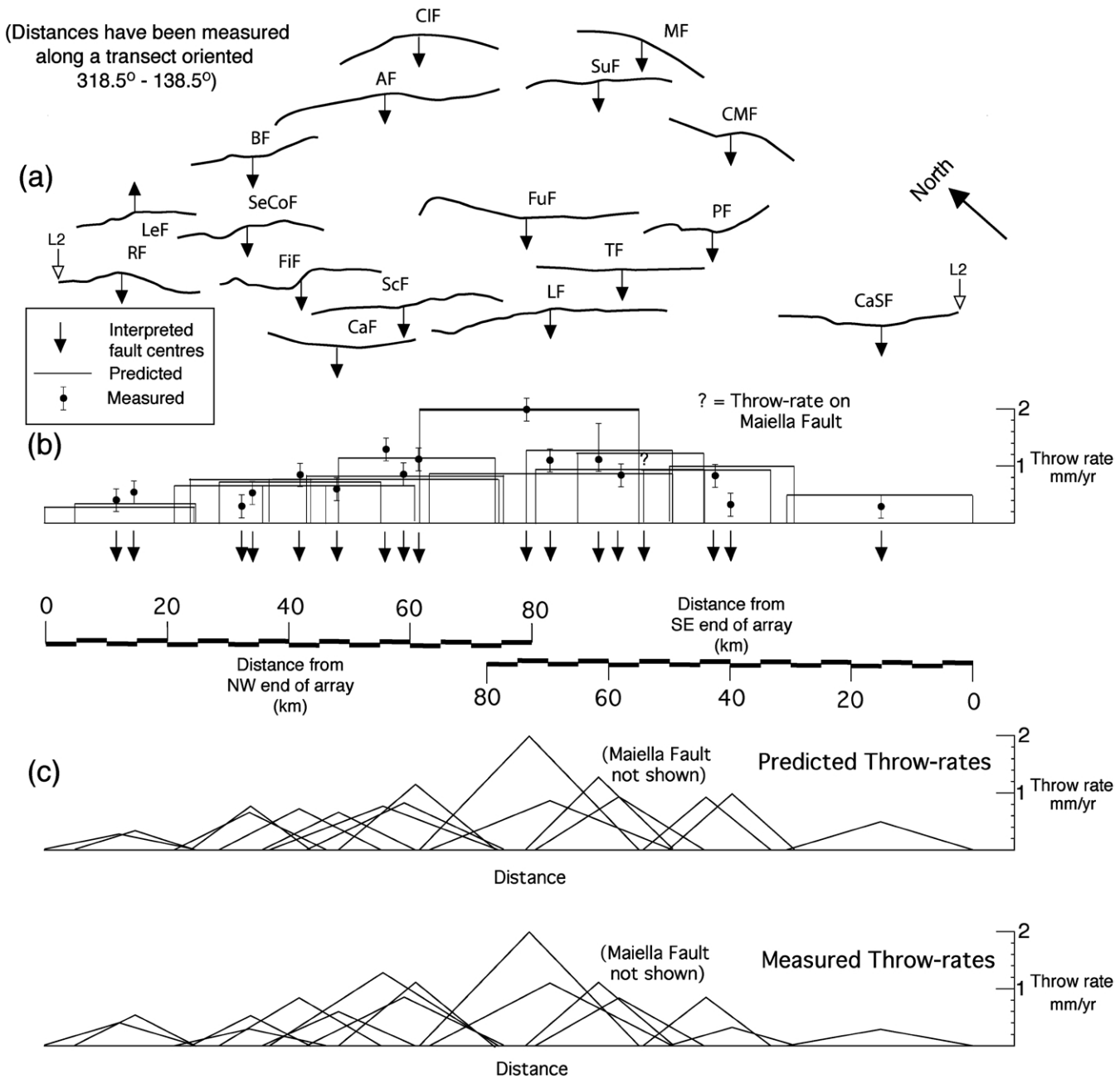

Fig. 3. Comparison of predicted and measured throw rates for the fault array in the Lazio–Abruzzo Apennines. The predicted rates have been calculated using the reasoning and method shown in Fig. 1 (see text for further explanation). Values are from Table 1. (a) Fault map, (b) throw-rate values, (c) throw profiles assuming linear throw-rate gradients. RF—Rieti Fault; LeF—Leonessa Fault; SeCoF—Sella di Corno Fault; FiF—Fiamignano Fault; BF—Barete Fault; AF—L'Aquila Fault; CIF—Campo Imperatore Fault; CaF—Carsoli Fault; ScF—Scurcola Fault; LF—Liri Fault; FuF—Fucino Fault; TF—Trassaco Fault; PF—Pescasseroli Fault; SuF—Sulmona Fault; MF—Maiella Fault; CMF—Cinque–Miglia Fault; CaSF—Cassino South Fault.

whole fault system) will grow in a non-self-similar fashion in order for its throw to achieve d_2, with throw-rates that are enhanced relative to more distal faults. We also use the method presented by Cowie and Roberts (2001) to deal with parallel active faults. For fault systems that have only recently acquired enhanced throw-rates on central faults due to a recent onset of fault interaction and throw profile readjustment, throws on central faults will not have achieved d_2 values, so fault spacing will still be close to x_1 (see Section 2). Above, we argue that the area we study contains such a fault system because parallel faults are active (Section 3) (Roberts and Michetti, 2003, this issue). If throw profile readjustment is due to elastic interaction through earthquake triggering, as argued by Cowie and Roberts (2001), rupture of a fault will reduce the stress on a fault that is parallel to it, making the second fault fail less often (Hodgkinson et al., 1996; Cowie, 1998); rupture of the second fault will have the same effect on the first fault. The result is that both faults will slip less often than an equivalent single fault because they will share the strain across this region. The effect will presumably be most marked when faults are closely spaced and their overlap is greatest. Unfortunately, we do not know exactly how one should modify the enhancement factors (E) determined from $2Ri/Li$ so as to deal with parallel active faults. This is because we do not know how to quantify the possible effects of details in the normal fault geometries or the crustal structure and rheology on strain partitioning in this or any region. We do not know exactly how any two parallel faults will share the strain. We suggest, following Cowie and Roberts (2001), that an approximation may be to multiply the enhancement factor for a fault by 0.5 if another fault is <15 km across strike (ca. half the average fault length) (see Willemse et al. (1996), Willemse (1997) and Cowie (1998) for the sizes of stress shadow zones relative to fault lengths), and overlaps by more than 50% of the two fault lengths. If two faults exist <15 km across strike and overlap by more than 50% of the fault lengths then the distributed deformation involves three faults and we multiply the enhancement factor by 0.33. This is certainly a potential source of error, and needs further work, but for now we use the above approximation.

Measured Ri and Li values were input into the relationship $E = 2Ri/Li$. The enhancement factors (E) were then modified by multiplying by 1, 0.5 or 0.33. The resultant values were normalised to the well-constrained maximum throw-rate for the Fucino Fault where both geomorphological and trench-site palaeoseismological observations suggest a throw rate of ca. 2 mm/yr (Roberts and Michetti, 2003, this issue) (Table 1; Fig. 3).

Overall, the predicted throw-rates compare well with the measured throw-rates (Table 1; Fig. 3). A six-fold increase in throw rates between distal and central faults is predicted, consistent with the measured six-fold increase (Roberts and Michetti, 2003, this issue) (Fig. 3). For the 16 active faults other than the Fucino Fault (to which we normalise other values), 14 have throw rates which fit with the prediction essentially within error of the measurements (± 0.2 mm/yr) whilst the other two faults have throw rates that are within 0.4 mm/yr of the measured values $\pm$ the measurement error.

The above results go some way towards validating the deformation rates proposed by Roberts and Michetti (2003, this issue). They suggest that the spatial pattern of throw rates is not unreasonable considering what we know of the scaling parameters of fault systems. The results also imply that the deformation rates of faults are controlled by the same factors which produce the global fault scaling relationship; $d = \gamma L$. We suggest that our results are consistent with throw profile adjustment due to elastic interaction associated with earthquake triggering (Cowie, 1998), but emphasise the fact that our results do not rely on elastic interaction. We suggest that the throw-rates measured over the last 18 kyrs may well be a good guide to the throw-rates for the next 18 kyrs because they are very similar to those predicted by scaling relationships, suggesting 18 kyrs is a long enough time period for a complete pattern of slip to emerge (compared with the incomplete slip-pattern recorded by historical earthquake catalogues spanning <1000 years).

Note that the throw-rates in the area we study appear to increase exponentially with distance along the array (Fig. 3), mainly due to the relatively-high throw-rate on the Fucino fault, yet we have used a linear function ($E = 2Ri/Li$) to calculate throw-rate enhancement. Note that the centrally-located Fucino Fault is isolated in space: there is no active fault within 15 km across strike which overlaps by more than 50% (Figs. 2 and 3); thus, unlike its neighbouring faults, the calculated throw rate is multiplied by 1 rather than 0.5 or 0.33, explaining our relatively high calculated rate, and perhaps the relatively high measured rate (Table 1). Thus, although we admit that there is an element of circular reasoning for this point, throw-rates on individual faults appear to be controlled by (1) the regional strain-rate, (2) their position within the array, and (3) their geometrical relationship with neighbouring faults as suggested by Cowie and Roberts (2001): our calculation method takes account of this.

5. Producing seismic hazard maps using measured rates and those predicted by fault scaling relationships

Above we have shown that the measured pattern of fault-slip over the last 18 ka is very similar to that predicted from fault scaling relationships, suggesting that the throw-rate database is not unreasonable. We now wish to see if the pattern of historical earthquake shaking for the region (INGV 1; Table 2) can be post-dicted using this throw-rate database. Our method is to combine fault throw-rates with (1) empirical data linking earthquake magnitudes, coseismic slip magnitudes and earthquake rupture lengths, (2) the

Table 2
Historical records of earthquake shaking and predicted shaking records for Lazio–Abruzzo (from INGV 1 and our own observations)

Town	Notes on total number of historical shaking events of all intensities	Dates of intensity ≥8.5 shaking events. Where shaking was equal to 8.5, this is indicated	Measured number of times shaken at intensity ≥8.5 since 1349 A.D.	Measured number of times shaken at intensity 9 (IX) since 1349 A.D.	Predicted number of times shaken at intensity 9 (IX) since 1349 A.D. from measured throw-rates (± error from ± 20% error on measured throw-rate)	Predicted number of times shaken at intensity 9 (IX) since 1349 A.D. from predicted throw-rates
1. Cittaducale	11 since 1315 A.D.	None	0	0	0 (+0/−0)	0
2. Pacentro	6 since 1349 A.D.	None	0	0	0 (+0/−0)	0
3. Rocca d'Evandro	4 since 1120 A.D.	None	0	0	0 (+0/−0)	0
4. Scanno	12 since 1349 A.D.	1706 A.D. (I. 8.5),	1	0	0 (+0/−0)	0
5. Anagni	9 since 1315 A.D.	None	0	0	0 (+0/−0)	0
6. Rieti	25 since 1298 A.D.	None in Catalogue but 1298 A.D. was intensity IX	0	0	1 +0/−0	1
7. Sulmona	21 since 1315 A.D.	1706 A.D.	1	1	1 (+0/−0)	2
8. Popoli	11 since 1456 A.D.	1456 A.D., 1706 A.D. (I. 8.5)	2	1	1 (+0/−0)	2
9. Sora	21 since 1349 A.D.	1349 A.D. (I. 8.5), 1654 A.D. (I. 8.5), 1915 A.D.	3	1	1 (+1/−0)	1
10. Pratola Pelinga	6 since 1456 A.D.	1456 A.D. (I. 8.5), 1706 A.D.,	2	1	1 (+0/−0)	2
11. Balsorano Vecchio	2 since 1349 A.D.	1349 A.D. (I. 8.5), 1915 A.D.	2	1	2 (+1/−0)	2
12. Pescosolido	4 since 1654 A.D.	1915 A.D.	1	1	1 (+1/−0)	1
13. Avezzano	14 since1349 A.D.	1349 A.D., 1915 A.D.	2	2	3 (+0/−1)	3
14. L'Aquila	35 since 1315 A.D.	1349 A.D., 1461 A.D., 1703 A.D.	3	3	2 (+0/−0)	1

Numbers for the towns relate to the numbers on Fig. 5e.

shapes and sizes of IX isoseismals on the Mercalli–Cancani–Sieberg (MCS) scale (within which horizontal ground accelerations exceed 0.5 gravity causing damage even to well constructed buildings) (Rieter, 1990; Keller and Pinter, 1996), and (3) attenuation/amplification functions for seismic shaking on bedrock compared to basin-filling sediments. The method and results we present are as follows (we describe them in more detail later after we have described our assumptions):

1. We have rasterised the geology of Lazio–Abruzzo from a 1:500000 geological map (Consiglio Nazionale delle Richerche, 1990) to produce a pixellated geology map within an Excel spreadsheet (Fig. 5a) with 2205 pixels. We wished to show to a first-order approximation, types of rock that might be associated with different shaking intensities during an earthquake. Thus, we differentiate only two types of geology and discuss this below: (a) Mesozoic/Neogene limestone and (b) Neogene–Recent foredeep (flysch) and extensional basin-filling deposits.
2. We have produced a map which shows maximum expected shaking intensities for each pixel (Fig. 5b). This is constructed through combining distances to active faults with the rasterised geology within Excel.
3. We show how many times localities receive enough energy to shake at intensities ≥IX in 18 kyrs by using measured throw-rates (Fig. 5c) and then calculated throw-rates (Fig. 5d): these maps assume homogenous bedrock geology, that is, they are not multiplied by Fig. 5a within Excel. The throw-rates are converted into earthquake shaking frequencies using the method described in Section 5.3 and Appendix A.
4. We multiply Fig. 5a by Fig. 5c, and then Fig. 5a by Fig. 5d within an Excel spreadsheet to produce Fig. 5e and f. These maps therefore include a seismic shaking attenuation/amplification function resulting from variations in the underlying geology and another related to distance from the epicentre and thus show how many times a locality is likely to shake at intensities ≥IX in 18 kyrs.

More detail concerning the assumptions and methods for the above are given in the following sections before we describe our results in detail.

5.1. Rupture dimensions and earthquake magnitudes

We wish to convert throw-rates into frequencies of earthquake shaking at specific sites of given intensity in a given time period. To do this we must choose an earthquake frequency–magnitude distribution and convert the throw in a given time period into a putative suite of earthquakes. This is a subjective process and below we explain our choices for the above. The reader should, however, bear in mind that ours in not intended to be a unique solution. Instead, we have sought to illustrate the worst-case scenario in terms of seismic shaking and seismic hazard.

The relationships between coseismic slip values, rupture lengths and earthquake magnitudes are relatively well known (Wells and Coppersmith, 1994; Mohammadioun and Serva, 2001). A Ms 6.5–6.9 normal faulting earthquake produces about 1 m of maximum throw with rupture lengths of about 15–20 km (e.g. Jackson et al. (1982) and Michetti et al. (1996) for the best constrained examples in the Mediterranean region). Thus, a 15 km long fault accumulating throw at 1 mm/yr could produce 18 m of throw in 18 kyrs by experiencing 18 Ms 6.5–6.9 earthquakes. Alternatively, throw could accumulate through occurrence of a Gutenberg–Richter or other earthquake magnitude–frequency relationship governing the relative numbers of small and large events (Gutenberg and Richter, 1944, 1954; Main, 1996). However, we have chosen to use only Ms 6.5–6.9 earthquakes to accommodate the throw. We do this because surface throw accumulation (that is, where we measure throw accumulation) will certainly be dominated by the large magnitude events because earthquakes with magnitude <ca. Ms 5.5 are unlikely to break the surface (Michetti et al., 2000). Indeed, earthquakes of magnitude <Ms 6.0 are usually poorly expressed at the surface as discontinuous traces or fractures showing inconsistent or no net throw and are characterised by much shorter surface ruptures than the source length defined by aftershocks (Bonilla et al., 1984; Darragh and Bolt, 1987; Bonilla, 1988; Slemmons et al., 1989). Ms 6.5–6.9 events are also probably a worst-case scenario for the Lazio–Abruzzo Apennines in terms of seismic hazards. Smaller earthquakes will produce less violent shaking and intensity values will probably not achieve intensity IX over large areas; larger earthquakes will probably occur less frequently so shaking at intensities ≥IX will have a long recurrence time compared with that produced by Ms 6.5–6.9 events. Thus, ca. Ms 6.5–6.9 events will produce damage at intensities ≥IX most frequently, which we consider here to be the worst-case for the Lazio–Abruzzo Apennines. Readers should keep this issue of earthquake magnitude distribution in mind when considering the implications of our results given below. The important point here is that because throw-rates vary spatially, so will the number of large magnitude earthquakes needed to produce the throw in a given time of period (e.g. 18 kyrs).

Note we choose to use surface rupture lengths (15 km) that are shorter than the lengths of the faults (20–40 km). We have done this because the 1915 Fucino earthquake did not rupture the entire length of the Fucino fault (Michetti et al., 1996). This is common, with all the recent large magnitude normal faulting earthquakes (>Ms 6.0) that are well studied in central Greece and Italy either rupturing in sub-events, and/or breaking only small parts (ca. 15–25 km or less) of longer faults (ca. 25–40 km) (1981 Gulf of Corinth: Roberts, 1996; 1980 Irpinia: Westaway and Jackson, 1987; 1894 Atalanti: Ganas et al., 1998; 1861

and 1995 Egion–Eliki: Roberts and Koukouvelas, 1996; Roberts and Ganas, 2000). Thus, rupture of short patches of the faults in Ms 6.5 earthquakes is not an unrealistic scenario and, as argued above, the choice of this magnitude maximises the long-term hazard.

5.2. Spatial distribution of seismic shaking and attenuation/amplification functions

The relationship between earthquake magnitude for shallow events and the geographic dimensions of regions subjected to given levels of shaking are fairly well-known, because isoseismal contours of given intensity have been measured for many earthquakes, including several large magnitude normal faulting earthquakes in central Italy (Grandori et al., 1991). The IX isoseismal is usually quasi-elliptical in shape. In Italy, the dimensions of such ellipses have been about 15 by 25 km across for Ms ca. 6.5–6.9 events (e.g. Postpischl, 1985; Galadini et al., 1995) (Fig. 4). The long axes of the ellipses are generally parallel to, and slightly longer than the surface rupture length. The centres of the ellipses are located close to the epicentres of the earthquakes, in the hanging walls of the dipping normal faults. The elliptical shapes are the result of the fact that (1) ruptures are linear in map view and have a finite length, and that (2) amplification of seismic energy occurs in Quaternary sediments infilling quasi-ellipse shaped extensional basins. However, for simplicity we assume circular patterns of energy release centred at the epicentres (25 km diameter circles for an energy level capable of producing shaking at intensities $\geq$IX), and discuss this in Section 5.8. In the calculations the circles needed for all the implied earthquakes are then attenuated/amplified by the Mesozoic bedrock/Tertiary–Quaternary sediments to produce spatial shaking event frequency distributions for intensities $\geq$IX.

Seismic attenuation/amplification functions related to the underlying geology are not well known for Lazio–Abruzzo because shaking has not been accurately measured for a large magnitude earthquake ($>$Ms 6.0) because no such earthquake has occurred since 1915. We suggest that there are basically three types of underlying geology in the portion of the Lazio–Abruzzo Apennines we consider: (1) Mesozoic–Neogene limestones; (2) Neogene foredeep-filling flysch; (3) extensional basin-filling Neogene–Quaternary deposits. In terms of the contrast between Mesozoic–Neogene limestones and Neogene–Quaternary deposits on historical isoseismal maps, we note that the isoseismal map for the 1915 earthquake shows a single intensity level decrease between localities on Mesozoic bedrock (A on Fig. 4) as opposed to Quaternary–Holocene basin-filling sediment (B on Fig. 4) at similar epicentral distances (e.g. around the town of Trassaco where a limestone ridge protrudes into the hanging wall basin to the Fucino Fault). We doubt that the isoseismals are very accurate in shape because the limestone ridge was certainly not densely or even sparsely populated in 1915 (steep slopes and cliffs exist which are unsuitable for building houses), so observations of shaking would have been very sparse or even inferred. However, the isoseismal map is the best we have so we should try to learn from it. In support of the isoseismal map, a number of houses pre-dating the 1915 event are still standing in Trasacco, a town that was almost destroyed in 1915 and now mostly consists of modern houses. The town is at about 680 m elevation, that is, right on the contact between the Neogene–Quaternary deposits filling the former Fucino lake-bed and the Mesozoic–Neogene limestone. The pre-1915 houses we identified have limestone forming part of their foundations or walls; they appear to be perched on small (<100 m^2), inliers of Mesozoic limestone. The surrounding houses appear not to be directly on limestone and their construction post-dates the earthquake. These qualitative observations, which certainly need more detailed study, support the notion that shaking on limestone was less severe than on Quaternary deposits to an extent that pre-1915 houses survived the 1915 earthquake when sited on Mesozoic limestone. Thus, we have adopted an attenuation/amplification function that decreases the intensity by a single value if two localities are equidistant from an epicentre, but one lies on Mesozoic or Neogene limestone and the other lies on extensional basin-filling Neogene–Quaternary deposits. Localities on Mesozoic and Neogene limestone never shake at intensities $\geq$IX in our model. In reality shaking at intensities $\geq$IX will occur close to the rupture trace even on Mesozoic and Neogene limestone, but these features will not be visible at the scale used on our shaking maps. This is consistent with the above shaking intensity observations around the Trasacco limestone ridge for the 1915 earthquake.

Our model allows localities on Neogene foredeep basin-filling sediments to shake in a similar manner to the Neogene–Quaternary extensional basin-filling sediments; that is, intensities $\geq$IX can occur if localities are within 12.5 km of an epicentre. Evidence for this comes from reported shaking intensities as high as X or XI on foredeep sediments during historical earthquakes in Lazio–Abruzzo and further south in the southern Apennines (Serva, 1994; Boschi et al., 1995; INGV 1). This is probably because localities on the Neogene foredeep-filling flysch are very susceptible to landsliding and such disturbed ground is probably responsible in part for the recorded high intensity shaking levels.

Note we have not calculated actual shaking values as fractions of gravitational acceleration, yet such values and how they attenuate with distance and bedrock type for a given magnitude are reasonably well-known for Europe (Ambraseys and Simpson, 1996; Ambraseys et al., 1996). To use this information, attenuation functions related to epicentral distance and bedrock type would have to be calculated for each pixel for each of the hundreds of implied earthquakes in the 18 kyrs time period considered. This was beyond the scope of this study but could be done in the future. However, we argue that the use of Mercalli intensity values and our simplistic attenuation functions are adequate for our purposes, which are to make a first attempt at

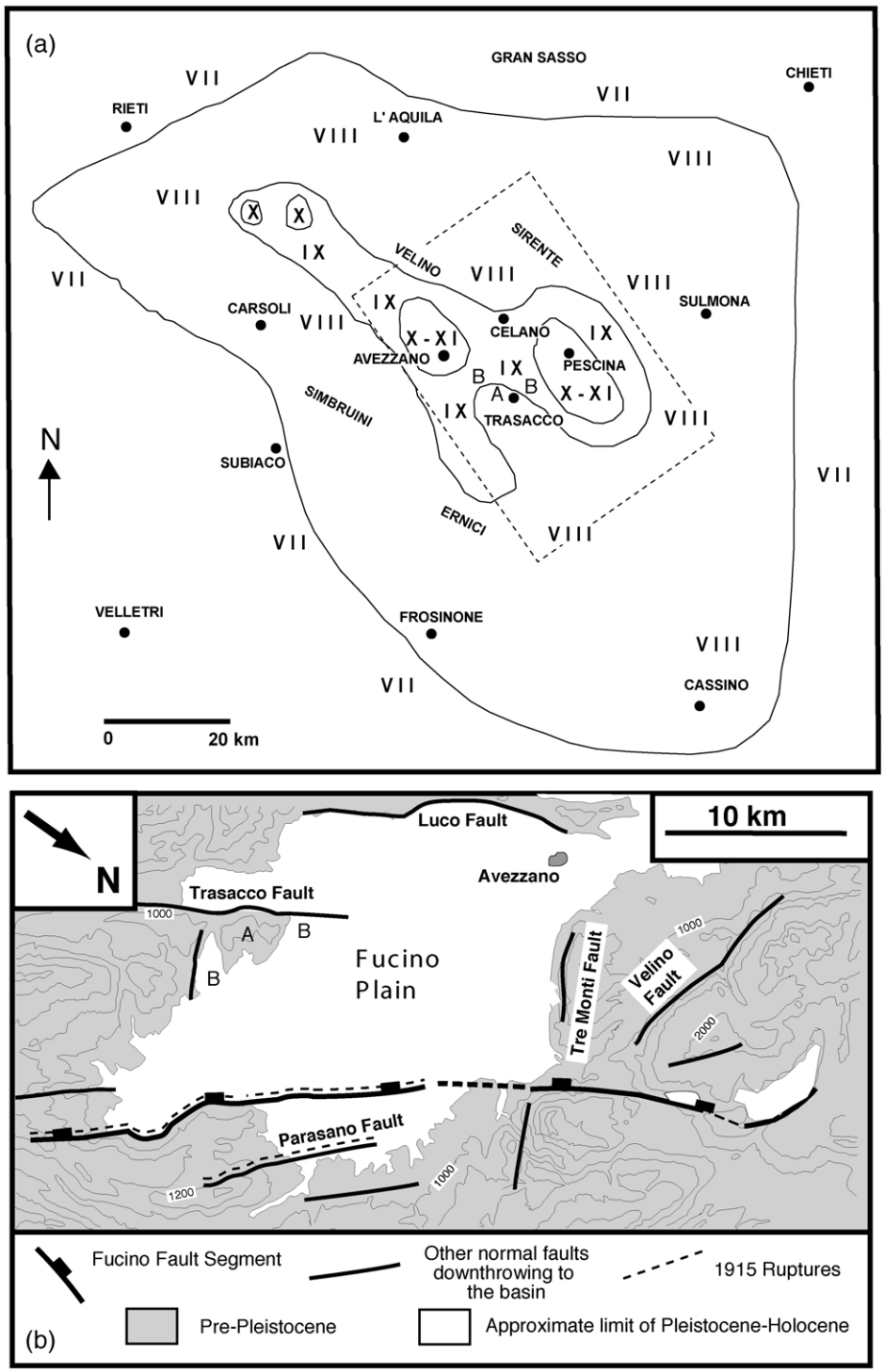

Fig. 4. Intensity distribution of the 13 January 1915 Ms ca. 6.9–7.0 earthquake of the Fucino Plain.

mapping the primary pattern of seismic hazard implied by spatial variation in fault throw-rates.

5.3. Converting throw-rates into earthquake frequencies

Using the above we can produce a map that shows how many times a locality receives enough energy to shake at ≥IX for the last 18 kyrs (that assumes only Ms 6.5–6.9 earthquakes). We do this by calculating the geographic distributions of localities that receive enough energy to shake at intensities ≥IX during single earthquakes, and then we sum and contour these distributions for the putative suite of Ms 6.5–6.9 earthquakes needed to produce the 18 kyrs pattern of throw.

The method is to fill up the area beneath distance versus throw-rate profiles (e.g. Fig. 3c) with earthquake ruptures

showing suitable dimensions for Ms 6.5–6.9 earthquakes (we use 1 m throw; 15 km length for such earthquakes). The method we use is explained in Appendix A. We simplify the procedure by assuming triangular throw-length profiles for the faults and ruptures, similar to those measured on well-constrained faults (Cowie and Shipton, 1998). The number of earthquakes required at different localities along the fault can then be calculated. We assume faults dipping at 45°, hypocentres at 10 km depth and 25 km diameter circular regions which receive enough energy to shake at intensities ≥IX centred on the epicentre.

There are errors associated with our map construction techniques. All our maps were produced using an Excel spreadsheet where one cell is a single pixel on the map. Our choice of rather large pixels (2.5 by 2.5 km), together with our use of the contouring algorithm in Excel has distorted the shapes of the map contacts between Mesozoic–Neogene Limestone and the Quaternary/Flysch. It has also produced an artificial-looking pixellated geology map (Fig. 5a). However, we were limited to these large pixel sizes because our manual counting method meant that it was not feasible to use more than 2205 pixels. This could be improved in future studies. Also, we have had to redraw the maps produced in Excel in a graphics package. This will have introduced a small spatial error. We estimate that faults, geological contacts and our hazard contours are within 1–2 km of their actual positions on maps showing an area of ca. 13,000 km^2.

5.4. Results concerning maximum expected shaking intensities

Fig. 5b shows the maximum expected shaking intensity for each of the 2205 pixels. The maximum intensity locations are defined by two factors: (a) the proximity to the nearest active fault (using a circle diameter of 25 km for an energy level capable of producing shaking at intensities ≥IX and of 50 km for that capable of producing shaking at intensities ≥VIII (Grandori et al., 1991); the epicentres are located 10 km from the fault trace in the hanging wall); and (b) the local bedrock geology (assuming that a Mesozoic–Neogene limestone site experiences one shaking intensity magnitude less than the Quaternary/Flysch sites). Note that this hazard map does not take account of any possible earthquakes that are not related to the active faults we have studied; possible alternative seismic sources are volcanism related deformation on the west coast of central Italy or sub-crustal earthquakes.

5.5. Frequency of shaking events calculated from measured throw rates

Fig. 5c shows how many times a locality could receive energy levels capable of producing shaking at intensities ≥IX in 18 kyrs. It uses the above method and assumes homogenous bedrock geology (i.e. a simple distance-related attenuation/amplification function). It demonstrates the effect of spatial throw-rate variation on the spatial pattern of seismic shaking. The map shows some remarkable features. First, a locality close to the centre of the Cassino fault receives enough energy to shake at intensities ≥IX only 5–10 times in 18 kyrs compared with the 115–120 times for a locality at the centre of the Liri fault in the same time period. This occurs because the former receives enough energy to shake at intensities ≥IX from only one relatively low throw-rate distal fault, whilst the latter is located in the hanging wall of four high throw-rate centrally-located faults and receives enough energy for intensities ≥IX from each of them. Second, in 18 kyrs, enough energy for shaking at intensities ≥IX arrives 115–120 times in the hanging wall of the Liri Fault, but only 5–10 times at a locality in the transfer zone between the Fucino and Fiamignano Faults. This variation occurs over a distance of only ca. 30 km and occurs despite the fact that the latter locality is situated close to the geographic centre of the fault array where one might expect relatively high earthquake shaking frequencies. This occurs because the latter locality is in the gap between three active faults and hence tens of kilometres from the central portions of the hanging walls of any active faults where most seismic energy, over long time periods, is released. Third, another area of low shaking frequency occurs in the footwall of the Fucino Fault because it overlaps with the L'Aquila and Sulmona faults by less than 50%, so no centre to a fault hanging wall is located in this region. Note that the Maiella Fault is not shown as an active fault on this map (compare with Fig. 5d) because at the time of writing we had poor data concerning its throw rate from our field studies although we suspect that it is an active fault (see Roberts and Michetti, 2003, this issue).

Clearly, the frequency of predicted seismic shaking events in the region varies both with distance along the overall fault array, but is also controlled by the fault geometries. Note that instead of the ca. six-fold increase in fault-specific throw rates (and presumably fault-specific earthquake frequencies) between distal and central faults in the array (see Fig. 3), we find a ca. 12-fold increase in the number of times a locality receives enough energy to shake

Fig. 5. Spatial variation in seismic hazards for Lazio–Abruzzo. (a) Bedrock geology map. Volcanic deposits exist in the southwest of the region but this does not affect our results. (b) Maximum expected intensities. (c) Number of times a region receives enough energy to shake at intensities ≥IX in 18 kyrs using measured throw-rates. (d) Number of times a region receives enough energy to shake at intensities ≥IX in 18 kyrs using predicted throw-rates (see Table 1). The method and reasoning are explained in Appendix A and the text. (e) Number of times a region shakes at intensities ≥IX in 18 kyrs using measured throw-rates and assuming a simple attenuation/amplification function where bedrock Mesozoic–Cenozoic Limestones shake at a single intensity level less than foredeep-extensional-basin-filling-sediments at the same epicentral distance. Numbers in circles locate the towns in Table 2. (f) Same as (e) but using predicted throw rates. Refer to Fig. 3 for fault names. Note, the Maiella fault is included in (d) and (f) but not (c) and (e).

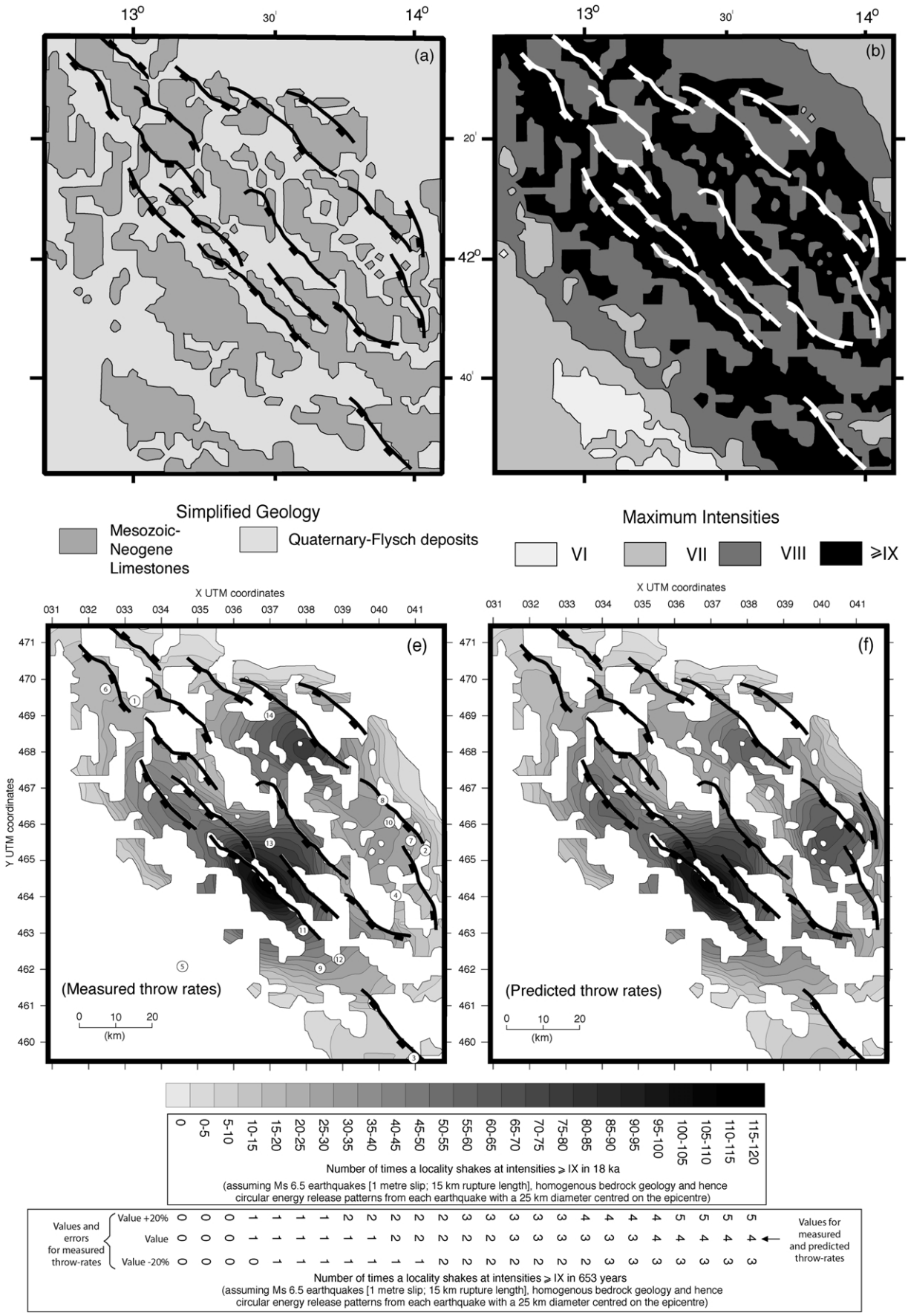
13°
30'
14°
(a)
(b)
20'
42°
40'
Simplified Geology
Mesozoic-Neogene Limestones
Quaternary-Flysch deposits
Maximum Intensities
VI
VII
VIII
≥IX
X UTM coordinates
031 032 033 034 035 036 037 038 039 040 041
Y UTM coordinates
471 470 469 468 467 466 465 464 463 462 461 460
(e)
(f)
(Measured throw rates)
(Predicted throw rates)
0 10 20
(km)
0 0-5 5-10 10-15 15-20 20-25 25-30 30-35 35-40 40-45 45-50 50-55 55-60 60-65 65-70 70-75 75-80 80-85 85-90 90-95 95-100 100-105 105-110 110-115 115-120
Number of times a locality shakes at intensities ≥ IX in 18 ka
(assuming Ms 6.5 earthquakes [1 metre slip; 15 km rupture length], homogenous bedrock geology and hence circular energy release patterns from each earthquake with a 25 km diameter centred on the epicentre)
Values and errors for measured throw-rates
Value +20%
Value
Value -20%
Values for measured and predicted throw-rates
Number of times a locality shakes at intensities ≥ IX in 653 years
(assuming Ms 6.5 earthquakes [1 metre slip; 15 km rupture length], homogenous bedrock geology and hence circular energy release patterns from each earthquake with a 25 km diameter centred on the epicentre)

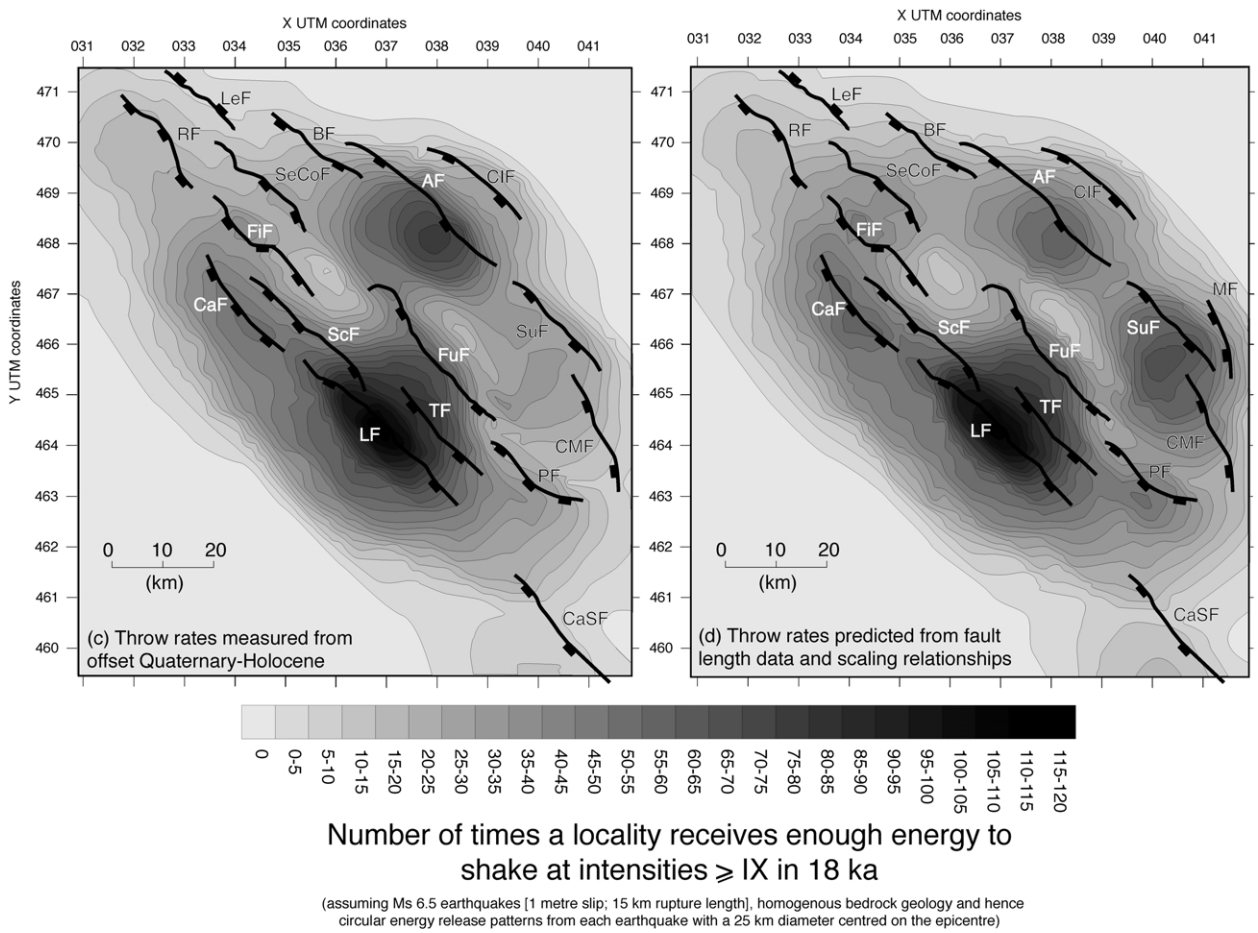

Fig. 5 (*continued*)

at intensities ≥IX (e.g. between the hanging walls of the Cassino and Liri Faults). This is because we use a 25 km diameter circle to denote the area which receives enough energy to shake at intensities ≥IX for each earthquake, and thus circles from neighbouring faults overlap. The 12-fold increase would decrease if a smaller diameter was used and increase for a larger diameter. We feel that 25 km is a reasonable value given the dimensions of IX isoseismals recorded from historical earthquakes in Central Italy (Grandori et al., 1991).

Note that the map can be converted to show the spatial variation in recurrence intervals for shaking and hence the spatial variation in probabilities of shaking within stated time periods. Thus, it shows the long-term shaking hazard, not where or exactly when the next earthquake will occur. Also, it is important to note that the map shows an energy-for-shaking-at-intensity-≥IX recurrence pattern rather than a fault-specific earthquake recurrence pattern.

5.6. Results from predicted throw-rates

Above we showed that the maximum throw-rates for each fault are well-predicted by scaling relationships using the equation $E = 2Ri/Li$. Thus, we can produce a map of how many times a locality receives enough energy for shaking at intensities ≥IX in 18 kyrs simply from input data on fault lengths, fault positions and fault array lengths (Fig. 5d; compare with Fig. 5c). We use the predicted throw-rates in Table 1. Again we have assumed triangular throw-rate profiles (Fig. 3c), constrained by the predicted maximum throw rate on each fault and assumed values of zero at the ends of each fault. Other than our use of predicted rather than measured throw rates, the method used is identical to that described for Fig. 5c. The map (Fig. 5d) shows very similar features to that from the measured throw rates (Fig. 5c). The main features are again (1) a ca. 10–12 fold increase in the number of times a locality receives enough energy to shake at intensities ≥IX in 18 kyrs between distal and central faults; (2) the low event frequency region in the transfer zone between the Fucino and Fiamignano faults; (3) the low event frequency region in the footwall of the Fucino Fault. The similarities are no surprise because the two independent throw-rate databases contain similar values. The main differences are as follows. Firstly, we note higher frequencies in the hanging wall of the Sulmona Fault: this occurs because the Maiella Fault, whose epicentres occur beneath the hanging wall of the Sulmona Fault in map view, is shown as an active fault on this map (Fig. 5d) but not on

the previous one (Fig. 5c) due to lack of data. Secondly, a lower event frequency is present in the hanging wall of the L'Aquila Fault because scaling relationships predict a lower throw-rate on the L'Aquila fault than we have measured from Quaternary/Holocene throw indicators. Thirdly, the actual values have changed elsewhere on the map (Fig. 5d) by $<5-10\%$ of the values on the previous map (Fig. 5c). Despite the above, we suggest that given our assumptions, there is very little difference between the maps showing values derived from measured as opposed to predicted throw-rates. We stress that the two maps are produced from independent data sources. However, the former is based on a detailed and time-consuming study of offset Quaternary/Holocene features in an area that is unusual for its exceptional preservation of such features (Roberts and Michetti, 2003, this issue), whereas the latter is based on analysis of fault map patterns.

5.7. Use of attenuation/amplification functions associated with the underlying geology

Finally, to produce shaking recurrence hazard maps for intensities $\geq$IX, we attenuate/amplify the potential shaking patterns (Fig. 5c and d) by multiplying shaking values in such a way as to reduce possible shaking by a single intensity value on Mesozoic–Neogene limestones (Fig. 5e and f). Thus, we only show the number of times a locality receives enough energy to shake at $\geq$IX in 18 kyrs for places where our attenuation/amplification functions allow such shaking (see Fig. 5b). Localities on Mesozoic–Neogene limestone never shake at intensities $\geq$IX in our model, except where they are on the rupture trace; this is not visible at the scale of Fig. 5. The map shows similar spatial variation in shaking frequencies to Fig. 5c and d, but emphasises locations where actual shaking at intensities $\geq$IX is likely.

5.8. Discussion of results

Our results suggest that there are large spatial variations in seismic shaking hazard across the region we study due to spatial variations in deformation rates. These variations occur across so-called 'Seismogenic Zones' that are assumed by others to have uniformly-distributed seismicity (e.g. Slejko et al., 1998). Although our many assumptions mean that the overall pattern of shaking is perhaps more relevant than the actual values shown on Fig. 5c–f, we argue that these maps reveal the primary pattern of seismic shaking hazard for the first time. The results could be improved by removing some of the assumptions we have used and we discuss this below.

It is a relatively simple matter to include different magnitude distributions such as a Gutenberg–Richter or other earthquake magnitude–frequency distributions (see Main (1996) for a review). However, the larger magnitude events ($>$ca. Ms 5.5) contribute all or the vast majority of throw accumulation on the fault at the surface (Michetti et al., 2000). Thus, adding smaller events into the included earthquake magnitude distribution will have little effect on the first order spatial pattern of earthquake shaking frequencies. If smaller magnitude events are included, the diameter of modelled regions that receive enough energy to shake at intensities $\geq$IX would decrease from the value of 25 km we use. The above amendments, if required, are simple tasks and could be attempted in a future study.

The circular patterns of energy release are not consistent with the fact that ruptures have a finite length; one could argue that ellipse shapes would produce more realistic results. However, (1) different rock types in the sub-surface will attenuate different amounts of energy, and (2) seismic energy will travel through different rock types—depending on travel paths—if the bedrock is heterogeneous (Chiarabba and Amato, 1994, 1997). Both of the above will produce non-circular and non-elliptical energy release patterns before the energy reaches the surface and is attenuated/amplified by the surface geology (e.g. Fig. 4). One would have to calculate the likely isoseismal shapes for each earthquake to improve the errors that are undoubtedly present in our results, using—as mentioned above—knowledge of attenuation functions associated with epicentral distance and underlying geology (e.g. Ambraseys and Simpson, 1996; Ambraseys et al., 1996). This would involve calculating the ground acceleration within each of the 2205 pixels for each of the hundreds of earthquakes that occur during an 18 kyr period; this was not feasible in our study. Nonetheless, we argue that although the detailed shapes of isoseismals for each earthquake have not been calculated the areas of isoseismals we use are consistent with the historical record; we believe that a poor choice of isoseismal area would produce a greater error in our results than a poor choice of the detailed shapes of isoseismals. Thus, again we suggest that the primary pattern of hazard is portrayed by our results.

We have used a very simple attenuation/amplification function related to the underlying geology, which produces only two shaking intensity levels (one on Mesozoic–Neogene limestones and one on sediments infilling foredeep/extensional basins) yet the geology is more complex in the Lazio–Abruzzo Apennines. In particular we have not differentiated between different types of basin-filling sediments yet alluvial fan, cemented scree, lake sediments, land prone to landslides and sediments altered by man will all shake at different values given the same energy input. There are few data on shaking levels on different rock types in Lazio–Abruzzo because the area has not been tested by a large magnitude earthquake since such measurements have been made routinely. We cannot simply extrapolate from smaller earthquakes because the relationship between shaking and earthquake magnitude is non-linear. Trifunac and Lee (1992) have shown that the average peak acceleration tends to increase slightly from sites on sediments to basement rock sites for intensities less than

VII; for VII and higher intensities, this trend is reversed with higher accelerations and peak displacements on sediment sites. Thus, we have used the simplest case where shaking of the Mesozoic bedrock is a single intensity level less than that on basin-filling sediments at the same epicentral distance. Unfortunately, it may be that our approach can only be improved if more data—including spectral acceleration data (see Slejko et al., 1998)—become available following a large magnitude earthquake in Lazio–Abruzzo. We realise that sensitivity analysis of the effects associated with the above uncertainties is desirable and this is planned for a future study.

Another issue is that of error propagation onto our hazard maps. Relative errors in measured throw-rates are produced by the amplitude of scarp height variation at some localities where end-glacial (ca. 18 ka) features are offset (Roberts and Michetti, 2003, this issue). Scarp height variation at given localities is about ±20%. Thus, for a scarp stated to have 18 m throw offsetting an 18 ka slope, the actual throw could be 21.6–14.4 m, and the implied throw-rate is therefore 1 ± 0.2 mm/yr. Errors are thus about ±20% and we have shown these on Fig. 5e and f (see Section 5.9). Absolute throw-rates could be higher if the scarps formed at 16 ka instead of 18 ka (see Roberts and Michetti (2003, this issue) for a discussion). However, as the age of the glacial maximum would be essentially synchronous across the region considered, the relative errors between localities on our maps would not change. The choice of 18 ka minimises the implied deformation rates. Also, the spatial variation (ca. 12-fold) is thus much larger than the relative error between localities. Errors also accrue due to the fact that we assume 1 m throw events. Predicted shaking frequencies would change if smaller or larger throw events were used, but we think 1-m-sized throw events are a reasonable value considering what is known about historical earthquakes in the region, and the fact that we attempt to constrain the worst case scenario. The assumption of circular energy release patterns will also induce errors as described above.

The above amendments will undoubtedly improve the seismic hazard maps, as will the inclusion of ground acceleration instead of intensity, but we argue that the first-order spatial variation in seismic hazard is conveyed by the maps in Fig. 5. We emphasise the point that the long time periods considered (18 ka from measured throw-rates and 10^5–10^6 million years provided by study of scaling relationships) means all the faults in the Lazio–Abruzzo Apennines will have ruptured numerous times so our hazard maps are most probably free of seismic gaps.

5.9. Comparison with the historical record of earthquake shaking

In order to check whether our results are realistic we have compared out post-dicted shaking frequencies with the historical earthquake shaking record since 1349 A.D., that is, 653 years (INGV 1) (see Section 1) (Table 2). We did not expect an excellent match between our post-dicted values and the measured values because fault-specific earthquake recurrence intervals constrained by palaeoseismology are ca. 500– > 3000 years (Section 1). We were particularly concerned that shaking frequencies around low throw-rate faults would be poorly sampled by the 653-year-historical shaking record. However, the frequency of shaking events at a given site is not governed by a single fault-specific recurrence interval, but rather by the cumulative shaking from slip on all nearby faults. Thus, we suspected that some evidence for spatial variations in shaking frequency might be present in site-specific shaking records, especially in the central part of the fault array where closely-spaced high throw-rate faults are located. It is also fortunate for this study that several towns located away from high throw-rate faults have records that are particularly detailed allowing us to be certain that recorded low event frequencies in these locations are real rather than due to poor record keeping (e.g. Rieti, Sora, Cittaducale and Anagni).

We found 14 towns out of the 48 that we examined that had numerous records of earthquake shaking back to around 1349 A.D.; their locations are plotted on Fig. 5e. Records for the 14 towns either included the 1349 A.D. earthquake, which produced shaking at intensities ≥IX, or in our estimation the towns were sufficiently developed in a cultural sense to have recorded a large magnitude event at this time, and subsequent to it, if such an event had occurred. We judge this by assessing whether low intensity events were also recorded at that site throughout the time period considered. We include on Fig. 5e a scale that allows the event frequency of ≥IX shaking in the 653 years since the 1349 A.D. event to be assessed and show errors induced by the ± ca. 20% error on measured throw-rates mentioned above. This scale is the same as the 18 kyrs scale normalised to 653 years and thus assumes that the rates of fault throw accumulation over long time periods (e.g. 18 kyrs) are representative of shorter time periods, thus deliberately ignoring the possibility of temporal earthquake clustering. The measured event frequency of shaking at intensities ≥IX from the historical record are compared with our post-diction in Fig. 6 (Table 2).

We find that the post-dicted shaking event frequencies from measured throw-rates compare reasonably well with those in the historical record. That we get a positive correlation at all is remarkable considering the short-time period we consider, the sensitivity induced by the high spatial resolution of our map, the number of assumptions we make during map construction, and the assumption of steady-state throw-rates. We also find that with the exception of the town of L'Aquila, shaking frequencies implied by predicted throw-rates are also similar to those in the historical record.

Another way to consider the results is that towns that do not fit the post-dicted shaking frequencies may be examples of sites that have experienced shaking frequencies that are genuinely above or below their long-term rates, that is, the

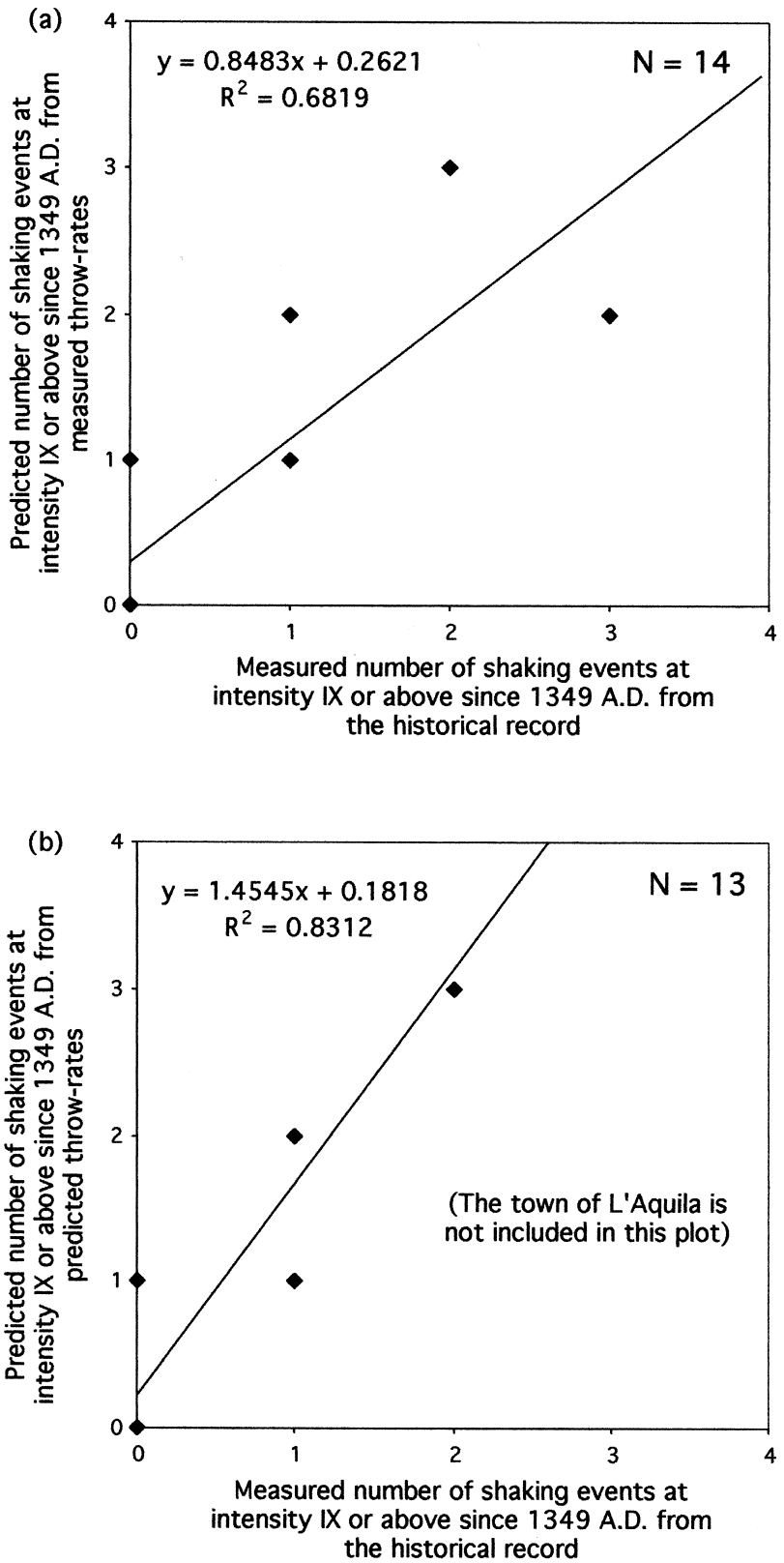

Fig. 6. Comparison of the historical record of earthquake shaking for the towns in Table 2 with the shaking frequencies predicted in Fig. 5e and f for the period 1349 A.D. to present. (a) Measured throw-rates. (b) Predicted throw rates.

effects of temporal earthquake clustering should be considered. The observation that the town of L'Aquila has had more earthquake shaking events than we post-dict from predicted throw-rates, and the L'Aquila fault has a post 18 ka throw-rate higher than we predict, may be consistent with the hypothesis of an earthquake cluster on this fault within the last 18 kyrs including the time period after 1349 A.D.; this intriguing result clearly needs further work. However, the underlying point is that comparing long-term throw-rates with short-term throw-rates should allow one to recognise earthquake clusters or anti-clusters, and this is facilitated by our method. Overall, we feel that the similarity between post-dicted and measured shaking frequencies provides some support for our approach, but realise that sensitivity analysis of the assumptions we use above is necessary to validate the results.

6. Discussion

In the seismic hazard maps produced herein, the number of times a locality receives enough energy to shake at intensities ≥IX, and hence the seismic hazard, varies over length scales governed by faults and the overall fault array. This spatial variation has not been revealed by more traditional seismic hazard maps based on combined instrumental and historical earthquake catalogues (e.g. Fig. 7) (see also Slejko et al., 1998). Our maps reveal this variation because they use every active fault as a seismic source rather than just those that have ruptured during the reliable portion of the combined historical and instrumental record (<ca. 1000 years).

This can be illustrated by considering how much fault-specific throw accumulates in 1000 years, a time period similar to the reliable portion of the historical record. For throw-rate values of 2 and 0.3 mm/yr, 2 and 0.3 m of throw accumulate in 1000 years. Thus, for a fault like the Fucino fault with a maximum throw-rate of 2 mm/yr, we would expect about two Ms 6.5 earthquakes in that position—if each produces about 1 m of throw—in 1000 years, a value that is similar to the measured value of three large (>Ms 6.0) earthquakes with metre-sized surface throw events in the interval 1915–550 A.D. (1365 years) interpreted by Michetti et al. (1996) in a trench investigation near the centre of the fault. However, for a fault like the Cassino Fault which has a maximum throw rate of only ca. 0.3 mm/yr, it is not surprising that Ms 6.5 events are not well-documented; that part of the fault would take 3333 years to accumulate enough elastic strain energy to produce a Ms 6.5 earthquake if that event produces 1 m of throw. Thus, localities with low throw-rates like that on the Cassino fault have a lower probability of being ruptured in the interval covered by the historical record (probability of 0.2 in 653 years) than localities on a high throw-rate fault like that on the Fucino fault (probability of 1.31 in 653 years). Thus, low throw-rate faults may well be under-represented on Fig. 7.

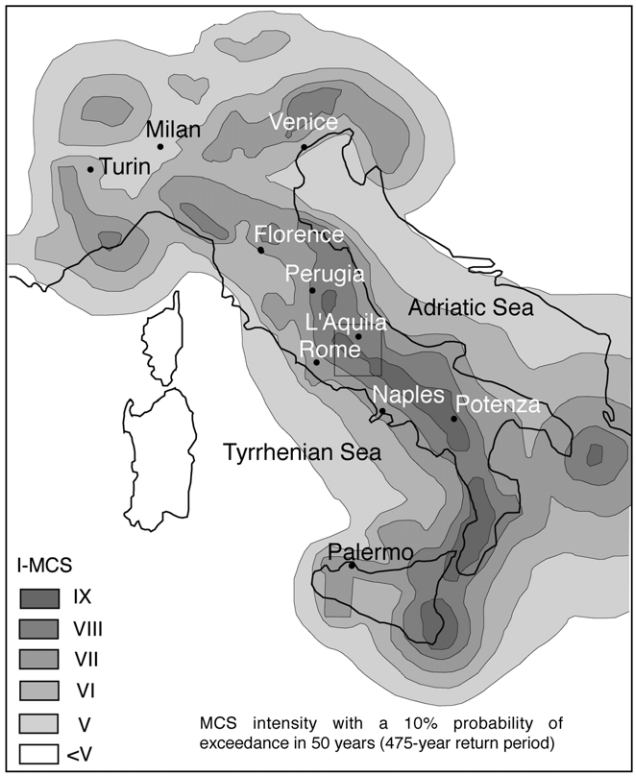

Fig. 7. Seismic hazard map for Italy based on seismicity data from GNDT 1 (1999). Box locates maps in Fig. 5.

We argue that the only way to realistically quantify hazard in the Lazio–Abruzzo Apennines and perhaps other settings where deformation rates are low, is to study how much throw (or slip) accumulates at different places over very long time periods. The time period must include numerous throw-increments at every location along the fault system. The throw-rate database of Roberts and Michetti (2003, this issue) seems to have achieved this. Prediction of seismic hazard using fault-scaling relationships also achieves this goal because it uses data concerned with the finite geometry of the fault system. Such geometries develop over a time period that includes hundreds to thousands of throw-increments at every location along the fault system.

Although above we suggest that realistic quantifications of hazard will only be achieved through study of long-term throw-rates, one could suggest that improving the historical record with more research might also help. Note that the 653 year measured shaking record for the 14 towns investigated above does seem to show spatial variation that is consistent with what we expect for faults whose throw-rates are controlled by evolution of their throw/length ratios (Cowie and Roberts, 2001) (Fig. 6b). This suggests that it might be possible to map and contour this record to make a shaking frequency map. However, in practical terms, it may well be unlikely that complete records for shaking for periods as long as 653 years will emerge for many more towns, yet many more towns with such records would be needed to

gain the spatial resolution of shaking event frequency achieved by our maps. Records longer than 653 years are preferable, yet such records for more towns are even less likely to be produced by historical research. Thus, realistically, our method may be the only pragmatic approach.

Thus, there is a new role for structural geologists in seismic hazard assessment. Measurements of the lengths, throws, map patterns and throw-rates of active faults can be used to constrain deformation rate patterns that emerge over time-spans covering numerous fault-specific seismic cycles. Such deformation rate databases can be converted to give measures of the spatial variation of seismic shaking event frequency and intensity across a region, and can therefore provide constraints on recurrence intervals for shaking and probability of shaking, and allow studies of temporal earthquake clustering.

7. Conclusions

We have used two independent data sets to produce seismic hazard maps for the Lazio–Abruzzo region, central Italy. Neither makes use of earthquake event frequency data from instrumental/historical seismicity because we believe that (1) such records for this region are too short for a full pattern of fault-slip to have emerged, especially near low throw-rate faults, and (2) too few towns have sufficient shaking records to allow spatial variation in shaking event frequency to be mapped with sufficient resolution. Our methods use the geologically-measured throw-rates since 18 ka and throw-rates predicted by fault scaling relationships (i.e. averaged over 10^5–10^6 years) to estimate how many 1-m-sized throw events are needed to produce the throw at different places along faults. Then, we sum isoseismal patterns for all the implied earthquakes to show the spatial variation in how many times localities receive enough energy to shake at intensities ≥IX in 18 kyrs. The long time intervals over which throw-rates are measured and calculated mean that it is unlikely that all the faults have not ruptured a number of times. Thus, our hazard maps are (1) most probably free of seismic gaps, and (2) are based on throw-rates that are likely to be representative of time periods that are very long compared with fault-specific earthquake recurrence intervals. The predicted throw-rate pattern matches the measured throw-rate pattern very closely. We successfully predict the (1) six-fold increase in throw-rates between distal and central faults in the array, (2) throw-rates on individual faults usually within the measurement error, and (3) the across strike spacing of active faults. The seismic hazard pattern resulting from both methods—with their assumptions which are detailed above—shows very high spatial resolution and compares well with the historical record of earthquake shaking. We reveal for the first time that one area in the centre of the region is likely to receive enough energy to shake at intensities ≥IX 115–120 times in 18 kyrs and neighbours an area only 30 km distant where this intensity of shaking could be achieved only 5–10 times over the same time period. Very similar hazard patterns are shown on maps produced by measured and predicted throw-rates. The second of our two methods produces predictions of fault throw-rates and hence hazard maps simply using the global scaling relationship between fault displacement (d) and lengths (L), $d = \gamma L$, and data concerning fault lengths, the map pattern of the fault array, and the maximum displacement value for one fault within that array. Thus, the method could be used rapidly in areas where such data are available, but deformation rate data are sparse. We argue that this type of calculation should be used routinely to validate deformation rate databases that are used to make seismic hazard assessments.

Finally, the pattern of seismic hazard in Lazio–Abruzzo where intensities ≥IX are spread over an across-strike distance of ca. 85 km will not be true of all active normal fault systems. We expect three types of active extensional fault system each with a different hazard pattern. One type is that described above in Lazio–Abruzzo where hazard increases towards the centre of the array and is spread across strike for a large distance. However, note that if the central fault achieves a throw value of d_2 then our calculations suggest that a single line of faults will accommodate the extension with other parallel faults ceasing in activity (see Section 3). A single line of faults can only produce ≥IX shaking over an across-strike distance of about 25 km. This is another type of fault system we expect. Examples of such localised active normal fault systems may include the Gulf of Corinth fault system, Greece and perhaps the Wasatch fault system, USA (see Cowie and Roberts, 2001). If the current throw-rates persist, the Fucino Fault will achieve d_2 and become one of these second types of fault system in 1.2 Ma, assuming a final $d_2 = \gamma L_2$ of $4.65 = 0.03 \times 155$, a throw-rate of 2 mm/yr and a current throw of 2.2 km. This will shut off the slip on faults parallel to it for a distance of 77.5 km in both directions across strike, as shown in Section 3. The last type of fault system we expect will be more juvenile and still in Stage 1 of the growth-linkage-interaction process (Fig. 1 of Roberts and Michetti, 2003, this issue). It is unclear whether such fault systems will show increasing throw-rates and hence seismic hazard towards the centre of the fault array. Future work will attempt to identify and study such a fault system.

The above emphasises the point that scaling relationships imply spatial and temporal changes in seismic hazards during the evolution of fault systems and these should be considered when producing seismic hazard assessments.

Acknowledgements

This study was funded by NERC GR9/02995 and

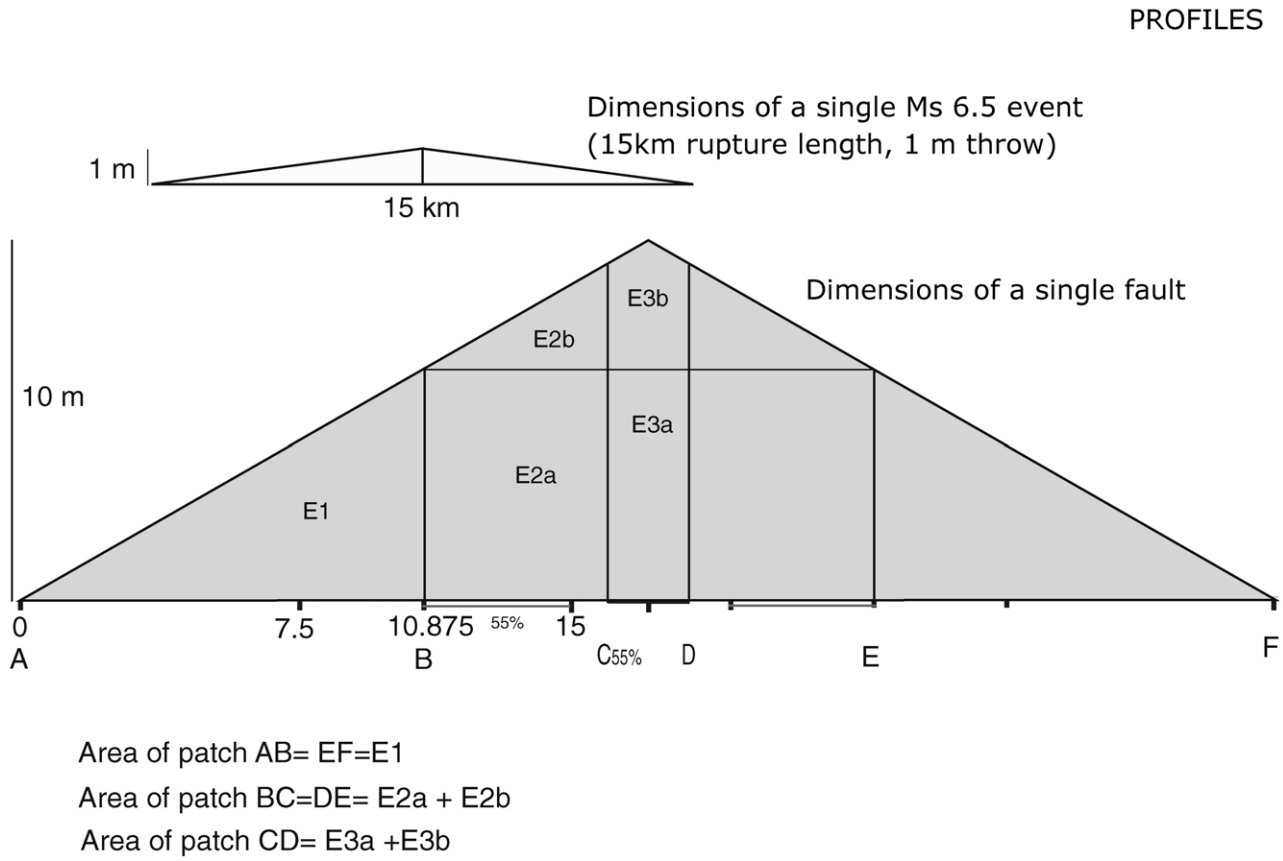

Fig. A1.

Birkbeck College (GPR), The Royal Society (PC), the State Scholarship Foundation of Greece (I.K.Y.) (IP), Benfield Greig Group plc. (GPR and IP) and ANPA (AMM). The Benfield Greig Hazard Research Centre at UCL is thanked for support. We thank Nigel Morewood, Leonello Serva and Eutizio Vittori for discussions concerning this paper. Jim Evans and several other anonymous referees are thanked for their comments.

Appendix A

We assume a triangular displacement profile for the faults and ruptures we model (Cowie and Shipton, 1998). We use the throw maximum accumulated in the last 18 kyrs and finite fault lengths for the faults (see Roberts and Michetti (2003, this issue) and Table 1) and 1 m coseismic throw to 15 km rupture length for ruptures (Jackson et al.,

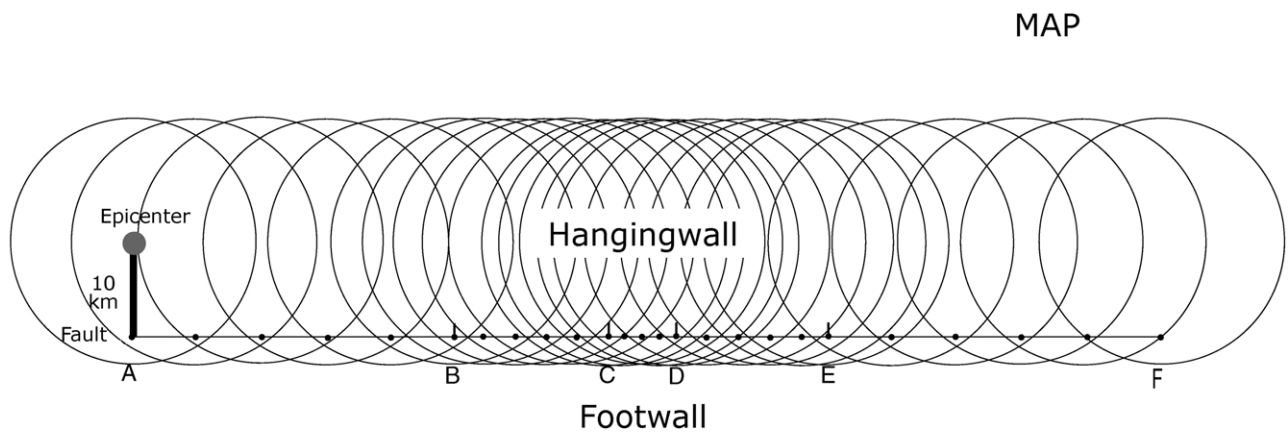

Fig. A2.

1982), assuming all surface throw accumulation is accomplished through ca. Ms 6.5 earthquakes. As a result, we can calculate (by comparing the areas of triangles for faults and ruptures) the number of earthquakes each fault experiences during 18 kyrs (Fig. A1).

Overall, the method we use is to (a) fill in the area of the fault triangle with ruptures, (b) extract the earthquake density along the fault, and (c) count, in map view (Fig. A2), the number of times each location around the fault experiences shaking at intensity IX or above, after locating the epicentres and 25 km circles denoting possible shaking at intensity IX or above.

In detail, the method first divides the fault into an odd number of patches according to its length. An odd number of patches are needed to produce maxima in throw at the fault centre. A fault of length (L) $15 < L < 30$ km is divided into three patches and a fault $30 < L < 45$ km into five patches. Each patch has a maximum length of 15 km, the same as that for a rupture. In the first case (three patches) we locate the centres of the two distal patches 7.5 km from both ends of the faults, and the third in the centre of the fault. In the second case (five patches) we set the three patches as previously and locate the centres of the other two about 15 km from both ends of the fault. Before we start counting the area, we define the boundaries (points B–E of the diagram Fig. A1) between the patches. We do not place these boundaries at exactly 50% distance between patches because patches closer to the centre of the fault accommodate more throw. The boundaries were located iteratively to produce the smallest error. In general, we found that a distance of 55% of the distance between the centres of the two neighbouring patches (point C to 15 km, point D to centre of the fault) measured away from the more central one gives the best result. This uneven spacing is necessary because the patches towards the fault centre experience more events than the distal ones; as a consequence they occupy more space. Then, we calculate the area of the triangles and rectangles using trigonometry (Fig. A2) to calculate the total area beneath the triangular displacement–length profile, and divide them by the equivalent area of an Ms 6.5 earthquake rupture. As a result, we know the number of events each patch contains and thus we can determine the earthquake density in each patch. Thereafter, we plot the epicentres 10 km away from the fault in the hanging wall (thus assuming 45° dipping faults and hypocentres at 10 km), add 25 km diameter circles which represent areas that receive enough energy to shake at intensities of IX and above, and finally count and contour the resulting values (Fig. A2). This method assumes that each patch has a homogeneous earthquake density, but in reality each patch includes more events towards the fault centre and less towards the fault tips. However, this makes little difference to our final conclusions.

References

Ambraseys, N.N., Simpson, K.A., 1996. Prediction of vertical response spectra in Europe. Earthquake Engineering and Structural Dynamics 25, 401–412.

Ambraseys, N.N., Simpson, K.A., Bommer, J.J., 1996. Prediction of horizontal response spectra in Europe. Earthquake Engineering and Structural Dynamics 25, 371–400.

Bonilla, M.G., 1988. Minimum earthquake magnitude associated with coseismic surface faulting. Bulletin of the Association of Engineering Geologists 25, 17–29.

Bonilla, M.G., Mark, R.K., Lienkaemper, X., 1984. Statistical relations among earthquake magnitude, surface rupture length, and surface fault displacement. Bulletin of the Seismological Society of America 68, 411–428.

Boschi, E., Favali, P., Frugoni, F., Scalera, G., Smriglio, G., 1995. Massima Intesita Macrosismica Risentita in Italia, Istituto Nazionale di Geofisica.

Chiarabba, C., Amato, A., 1994. From tomographic images to fault heterogeneiities. Annali di Geofisica XXXVII, 1481–1494.

Chiarabba, C., Amato, A., 1997. Upper crustal structure of the Benevento area (southern Italy): fault heterogeneities and potential for large earthquakes. Geophysical Journal International 130, 229–239.

Clarke, P.J., Davies, R.R., England, P.C., Parsons, B.E., Billiris, H., Paradissis, D., Veis, G., Denys, P.H., Cross, P.A., Ashkenazi, V., Bingley, R., 1997. Geodetic estimate of seismic hazard in the Gulf of Korinthos. Geophysical Research Letters 24, 1303–1306.

Consiglio Nazionale delle Ricerche (CNR), 1990. Structural model of Italy, 1:500000. S.E.L.C.A. Florence.

Cowie, P.A., 1998. A healing-reloading feedback control on the growth rate of seismogenic faults. Journal of Structural Geology 20, 1075–1087.

Cowie, P.A., Roberts, G.P., 2001. Constraining slip rates and spacings for active normal faults. Journal of Structural Geology 23, 1901–1915.

Cowie, P.A., Shipton, Z.K., 1998. Fault tip displacement gradients and process zone dimensions. Journal of Structural Geology 20, 983–997.

Darragh, R.B., Bolt, B.A., 1987. A comment on the statistical regression relation between earthquake magnitude and fault rupture length. Bulletin of the Seismological Society of America 77, 1479–1484.

Galadini, F., Galli, P., Giraudi, C., Molin, D., 1995. Il terremoto del 1915 e la sismicita della piana del Fucino (Italia Centrale). Boll. Soca. Geol. It. 114, 635–663.

Galadini, F., Galli, P., Giraudi, C., 1997. Geological investigations of Italian earthquakes: new paleoseismological data from the Fucino Plain (Central Italy). Journal of Geodynamics 24, 87–103.

Ganas, A., Roberts, G.P., Memou, T., 1998. Segment boundaries, the 1894 ruptures and strain patterns along the Atalanti Fault, Central Greece. Journal of Geodynamics 26, 461–486.

Giraudi, C., Frezzotti, M., 1995. Paleoseismicity in the Gran Sasso Massif (Abruzzo, Central Italy). Quaternary International 25, 81–93.

GNDT 1, 1999. Hazard Maps. http://www.dstn.it/ssn/PROG/2000/carte_pericolosita/mcs_e.gif.

Grandori, G., Drei, A., Perotti, F., Tagliani, A., 1991. Macroseismic intensity versus epicentral distance: the case of Central Italy. Tectonophysics 193, 165–171.

Gutenberg, B., Richter, C., 1944. Frequency of earthquakes in California. Bulletin of the Seismological Society of America 34, 186–188.

Gutenberg, B., Richter, C., 1954. The Seismicity of the Earth and Associated Phenomena, Princeton University Press, Princeton, New Jersey, pp. 1–310.

Hodgkinson, K.M., Stein, R.S., King, G.C.P., 1996. The 1954 Rainbow Mountain–Fairview Peak–Dixie Valley earthquakes: a triggered normal faulting sequence. Journal of Geophysical Research 101, 25459–25471.

INGV 1. Istituto Nazionale di Geofisica e Vulcanologia. Catalogue of strong Italian earthquakes from 461 B.C. to 1990 A.D. http://80.117.141.2/cft/).

Jackson, J.A., Gagnepain, J., Houseman, G., King, G.C.P., Papadimitriou, P., Soufleris, C., Virieux, J., 1982. Seismicity, normal faulting, and the geomorphological development of the Gulf of Corinth (Greece): the Corinth earthquakes of February and March 1981. Earth and Planetary Science Letters 57, 377–397.

Keller, E.A., Pinter, N., 1996. Active Tectonics, Prentice Hall, New Jersey, ISBN-0-02-304601-5, 338pp.

Kostrov, V., 1974. Seismic moment and energy of earthquakes, and seismic flow of rock. Izv. Acad. Sci. USSR Phys. Solid Earth 1, 23–44.

Machette, M.N., Personius, S.F., Nelson, A.R., Schwartz, D.P., Lund, W.R., 1991. The Wasatch fault zone, Utah—segmentation and history of Holocene earthquakes. Journal of Structural Geology 13, 137–149.

Main, I., 1996. Statistical physics, seismogenesis, and seismic hazard. Reviews of Geophysics 43, 433–462.

Michetti, A.M., Brunamonte, F., Serva, L., Vittori, E., 1996. Trench investigations of the 1915 Fucino earthquake fault scarps (Abruzzo, Central Italy): geological evidence of large historical events. Journal Geophysical Research 101, 5921–5936.

Michetti, A.M., Ferreli, L., Esposito, E., Porfido, S., Blumetti, A.-M., Vittori, E., Serva, L., Roberts, G.P., 2000. Ground effects during the 9 September 1998, $M_w = 5.6$, Lauria earthquake and the seismic potential of the "Aseismic" Pollino region in Southern Italy. Seismological Research Letters 71, 31–46.

Mohammadioun, B., Serva, L., 2001. Stress drop, slip type, earthquake magnitude and seismic hazard. Bulletin of the Seismological Society of America 9 (4), 694–707.

Nicol, A., Walsh, J.J., Watterson, J., Underhill, J., 1997. Displacement rates of normal faults. Nature 390, 157–159.

Pantosti, D., D'Addezio, G., Cinti, F., 1996. Paleoseismicity of the Ovindoli–Pezza fault, central Apennines, Italy: a history including a large, previously unrecorded earthquake in the Middle Ages (860–1300 A.D.). Journal of Geophysical Research 101, 5937–5960.

Postpischl, D. (Ed.), 1985. Atlas of isoseismal maps of the Italian earthquakes. C.N.R., Quaderni de "La Ricerca Scientifica", 114(2A), 164pp.

Rieter, L., 1990. Earthquake Hazard Analysis: Issues and Insights, Columbia University Press, New York, 254pp.

Roberts, G.P., 1996. Noncharacteristic normal faulting surface ruptures from the Gulf of Corinth, Greece. Journal of Geophysical Research 101, 25255–25267.

Roberts, G.P., Ganas, A., 2000. Fault-slip directions in central-southern Greece measured from striated and corrugated fault planes: comparison with focal mechanism and geodetic data. Journal of Geophysical Research 105, 23,443–23,462.

Roberts, G.P., Koukouvelas, I., 1996. Structural and seismological segmentation of the Gulf of Corinth fault system: Implications for models of fault growth. Annali di Geofisica XXXIX, 619–646.

Roberts, G.P., Michetti, A.M., 2003. Spatial and temporal variations in growth rates along active normal fault systems: an example from The Lazio–Abruzzo Apennines, central Italy. Journal of Structural Geology, doi:10.1016/S0191-8141(03)00103-2.

Schlische, R.W., Young, S.S., Ackermann, R.V., Gupta, A., 1996. Geometry and scaling relations of a population of very small rift-related faults. Geology 24, 683–686.

Serva, L., 1994. The effects on the ground in the intensity scales. Terra Nova 6, 414–416.

Slejko, D., Peruzza, L., Rebez, A., 1998. Seismic hazard maps of Italy. Annali di Geofisica 41, 183–214.

Slemmons, D.B., Bodin, P., Zang, X., 1989. Determination of earthquake size from surface faulting events, Proceedings of the International Seminar of Seismic Zonation, Guangzhou, China, State Seismological Bureau, Beijing, p. 13.

Trifunac, M.D., Lee, V.W., 1992. A note on scaling peak acceleration, velocity and displacement of strong earthquake shaking by Modified Mercalli Intensity (MMI) and site soil and geologic conditions. Soil Dynamics and Earthquake Engineering 11, 101–110.

Wells, D.L., Coppersmith, K.J., 1994. New empirical relationships among magnitude, rupture length, rupture width and surface displacement. Bulletin of the Seismological Society of America 84, 974–1002.

Westaway, R., Jackson, J., 1987. The earthquake of 1980 November 23 in Campania–Basilicata (southern Italy). Geophysical Journal of the Royal Astronomical Society 90, 375–443.

Willemse, E.J.M., 1997. Segmented normal faults: correspondence between three-dimensional mechanical models and field data. Journal of Geophysical Research 102, 675–692.

Willemse, E.J.M., Pollard, D.D., Aydin, A., 1996. Three-dimensional analysis of slip distributions on normal fault arrays with consequences for fault scaling. Journal of Structural Geology 18, 295–309.